RESEARCH ACTIVITIES

PHOTOFRAGMENT POLARIZATION SPECTRUM OF HCN

Takashi NAGATA, Tamotsu KONDOW, and Kozo KUCHITSU
Department of Chemistry, Faculty of Science, The University of Tokyo, Bunkyoku, Tokyo 113, Japan

Atsunari HIRAYA and Kosuke SHOBATAKE
Institute for Molecular Science, Myodaiji, Okazaki 444, Japan

Polarization of the fluorescence from the excited fragments produced by molecular photodissociation process provides valuable information as follows, 1) the sign of polarization reveals the symmetry of the photo-excited, the precursor, and/or the fragment emitting state, 2) the magnitude of polarization reflects the nature of the dissociation process such as the branching ratio of the direct to the predissociation process and/or the lifetime of the precursor state. A photofragment polarization spectrum of HCN has been measured in the wavelength region of 105-125nm by means of SOR light as a polarized, tunable VUV light source.

Figure 1 shows a schematic drawing of the present setup of the polarimeter and the timing chart of the photon counting system. The monochromatized SOR light, linearly polarized along the X axis, is incident along the Z axis into a sample cell. Partially polarized fluorescence from the excited photofragment is viewed along the Y axis through the optics of the polarimeter. A photoelastic modulator (PEM) is oriented with its optical axis 45° relative to the X axis. In this setup the PEM rotates the plane of polarization of X- or Z- polarized light by 90° about Y axis, at maxima and minima of the retardance curve, while transmits light without such effect at zero-crossings points of that curve. As the passing axis of the polarizer

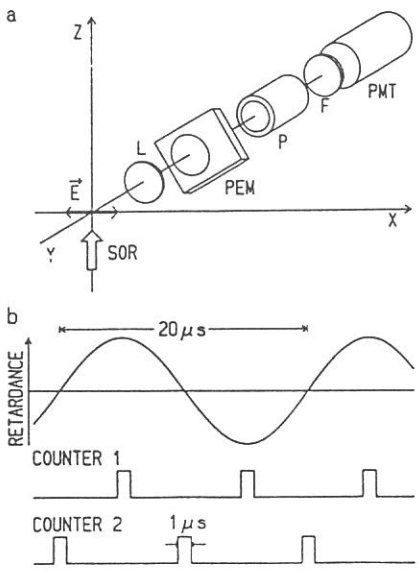

Figure 1. A schematic drawing of experimental setup and timing chart.

after PEM is parallel to the Z axis, counter 1 gated at maxima and minima of retardation counts only the photons of the X-polarized light. Inversely, counter 2 only counts the photons of the Z-polarized light. In this manner, intensities of the parallel (I_X) and the perpendicular (I_Z) component, with respect to the polarization axis of the excitation light, are measured separately for the partially polarized fluorescence. The degree of polarization (P) given as $(I_X-I_Z)/(I_X+I_Z)$ is recorded as a function of the excitation wavelength.

Figure 2 shows the absorption, fluorescence excitation, and photofragment polarization spectra (PPS) of HCN at 105-125 nm. A filled circle in the figure represents the degree of the fluorescence polarization measured by Nagata et al.[1] at 121.6 nm by means of an unpolarized Lyman-α radiation. The degree of polarization at 121.6 nm in the present work (0.046 ± 0.005) is in very good agreement with the previous value (0.045 ± 0.010). According to Nagata et al. the excited state should be $^1A'$ of bent geometry in this wavelength region, since P is always positive in this region. Regarding the absolute value, P varies slowly with the excitation wavelength between 105 and 116 nm with maximum value (0.077) at around 112.5 nm. This implies that the photodissociation in this region is predissociative as P is lower than the limiting value (1/7) for direct dissociation. Above 116 nm two minima are clearly observed at 119.0 nm and 112.4 nm, the former coincides with an absorption maximum, while the latter does not coincide with any absorption peak but with a peak of the fluorescence excitation spectrum. The origin of this behavior of P is now being examined.

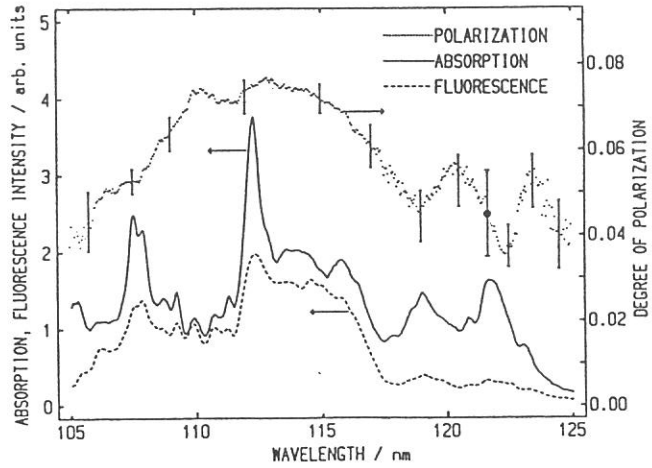

Figure 2. Absorption, fluorescence excitation, and photofragment polarization spectra of HCN.

1) T. Nagata, T. Kondow, Y. Ozaki and K. Kuchitsu, Chem. Phys. Lett. 81 (1981) 391.

VUV ABSORPTION AND FLUORESCENCE EXCITATION SPECTRA OF DIMERS AND CLUSTERS OF Xe IN A SUPERSONIC FREE JET

Atsunari HIRAYA and Kosuke SHOBATAKE

Institute for Molecular Science, Myodaiji, Okazaki 444, Japan

In contrast to the electronic structure of rare gas dimers which have been extensively studied, potential curves of rare gas clusters are not well known especially in those excited states. As a first step of the studies on rare gas clusters, direct absorption and fluorescence excitation spectra have been measured in a supersonic free jet of Xe. Figure 1 shows the absorption spectra measured in a supersonic free jet of neat Xe gas, at stagnation pressures of 460 and 760 torr, in the wavelength region 105 - 160 nm. In addition to the atomic lines and Xe_2 bands which are already known, several new features are seen in the spectra. A most conspicuous feature is an intense and broad band observed at the longer wavelength side of the lowest allowed atomic line $^3P_1$ (146.96 nm). Figure 2 shows the absorption and fluorescence excitation spectra measured in the wavelength region near this atomic line, at several stagnation pressures. Absorption bands at 146.4nm and 148.2nm (in the spectra at 200torr) are due to the Xe dimer, and are assigned respectively as the transitions to the 1_u(repulsive) and 0_u^+(bound) excited states, both of which correlate to $^3P_1+^1S_0$. With increasing stagnation pressure, the peak position of

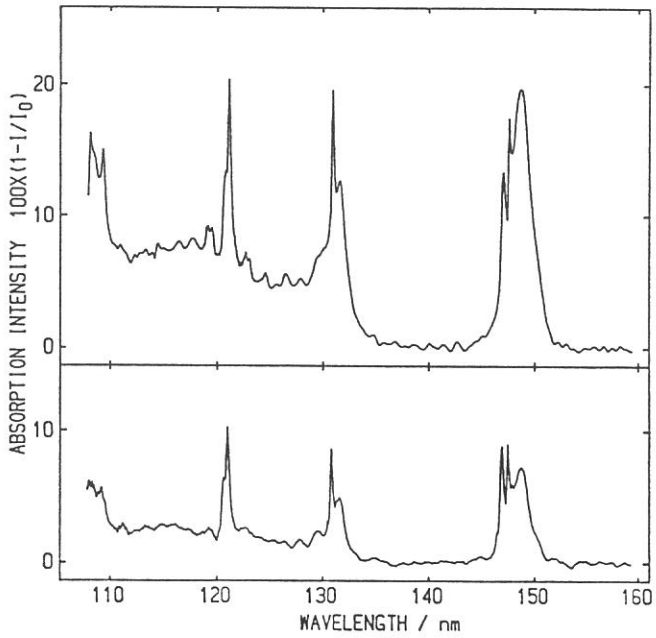

Figure 1. Absorption spectra of a supersonic free-jet of Xe.

the red-side band shifts toward the blue side and reaches 147.8 nm at 770 torr. A stagnation pressure dependence of the absorption intensity at 147.8nm was found nearly cubic, while those at the atomic line and at the 1_u band of Xe_2 are approximately linear and square, respectively. These findings lead us to the assignment that the broad absorption band at 147.8 nm is due to the Xe_n clusters. In the fluorescence excitation spectra monitored at longer wavelengths than 180 nm, one can find only one broad band which almost exactly follows the broad absorption profile. Because the wavelengths of the monitored light is longer than 180 nm, only the excitation transitions to the state which form the emitting states in the longer wavelength than 180 nm contribute to the fluorescence excitation spectra. Although the simplest assignment for the emitting state is given as the bound excited states of the Xe clusters, an alternative assignment as the bound excited states of Xe_2 formed by the dissociation of Xe clusters is also probable. For both emitting states, however, the initially prepared states are those of Xe clusters. Therefore, present fluorescence excitation spectra can be regarded as the excitation function of Xe cluster(s). As a conclusion, the absorption band which extends from 144nm to 151nm peaking at 147.8nm (at 770 torr) is assigned as the cluster band(s). The location of this cluster band is in good agreement with the lowest energy absorption band at 148.3nm observed for solid Xe.

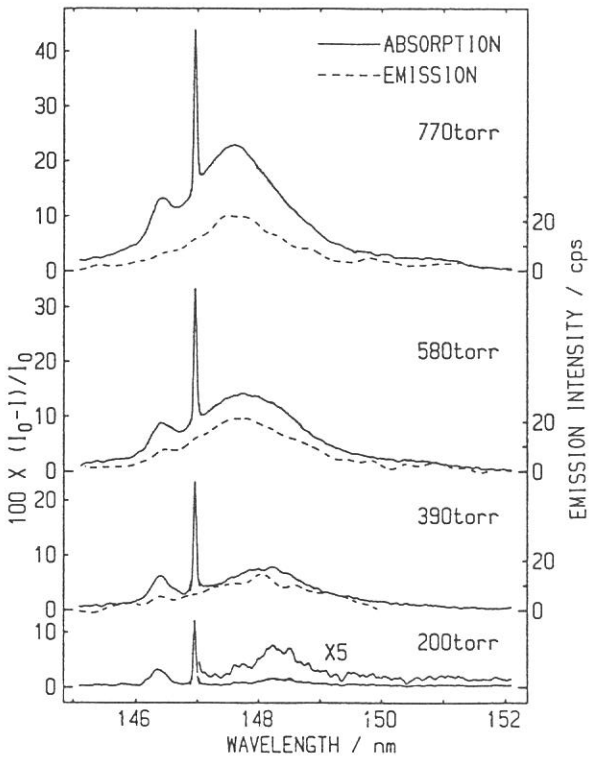

Figure 2. Absorption and fluorescence excitation spectra of a supersonic free-jet of Xe.

VUV ABSORPTION AND FLUORESCENCE EXCITATION SPECTRA OF JET-COOLED I_2

Atsunari HIRAYA, Kosuke SHOBATAKE, and Robert J. DONOVAN*

Institute for Molecular Science, Myodaiji, Okazaki 444, Japan
*Department of Chemistry, University of Edinburgh, West Mains Road, Edinburgh EH9 3JJ, UK

Direct absorption and fluorescence excitation spectra of I_2 seeded in a supersonic free jet of He have been measured simultaneously in the wavelength region of 174.5 - 193nm as shown in Figure 1(a). Comparing with the spectra (b) obtained for room temperature vapor, vibrational cooling in free jet is indicated as: i) decreasing in intensity of vibrational hot-band in the C_6 Rydberg system, ii) narrowing of the vibrational envelope in the D ion-pair system. Comparing these spectra, it can be concluded for the fluorescence dips in D ion-pair system that: 1) The dip at 185nm, which appeared only for vapor phase spectra, results from an overlap of Franck-Condon patterns of each transitions from v"=0, 1, 2, ··· in the ground state, 2) The dip at 182.5nm, observed for both spectra, results from a crossing of the dissociative potential curve with that of D ion-pair state, 3) Since the dips at 174-178nm fade out for the spectrum in a jet, the contribution of the hot-band transitions for these dips is found to be fairly large. This finding confirms our previous proposal that the isoenergetic perturbations between the vibronic levels of the C_6 Rydberg state and those of the D ion-pair state are the origin of the dips at 174-178nm.

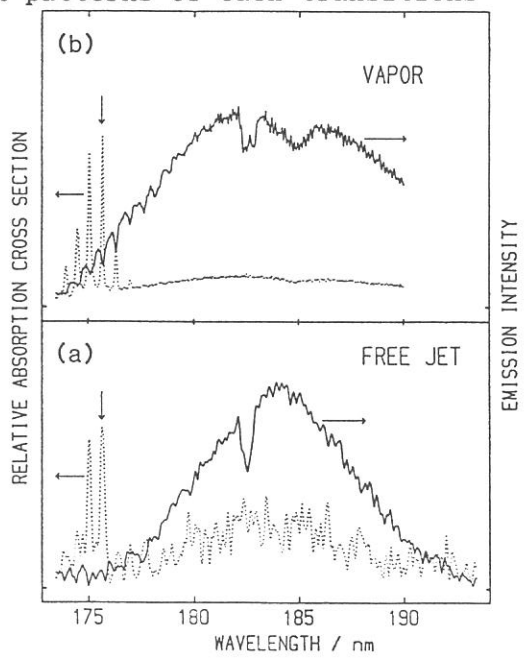

Figure 1. Absorption and fluorescence excitation spectra of I_2 in a supersonic free-jet (a), and in a gas cell (b).

ABSORPTION AND FLUORESCENCE EXCITATION SPECTRA OF N_2O AND CS_2 IN SUPERSONIC FREE JET

Ikuo TOKUE, Atsunari HIRAYA*, and Kosuke SHOBATAKE*

Department of Chemistry, Niigata University, Niigata 950-21
*Institute for Molecular Science, Myodaiji, Okazaki 444

Photoabsorption and photochemical processes of CS_2 and N_2O in the VUV region have been the subject of numerous investigations during the past half century. Despite these efforts, the Rydberg state assignments of CS_2 by various investigators are not consistent. As for N_2O, fluorescence excitation spectra are affected by the NO β band which was produced by secondary reactions[1]. In the gas phase, a supersonic free jet technique combining with SOR as a light source provides rotationally and/or vibrationally cooled spectra in the VUV region.

We report here preliminary results of the measurement of absorption cross section (c.s.) and fluorescence excitation spectra (e.s.) of N_2O and CS_2 in a free jet. In the present measurement, CS_2 vapor at room temperature was mixed with He carrier gas and expanded at a stagnation pressure of 220 torr through an orifice. Although expansion conditions and diluent gas composition were not adjusted, jet-cooling effects were recognized on comparing with the spectra reported by Hemley et al.[2] N_2O gas was expanded at a stagnation pressure of 200-780 torr. The light transmitted by the sample was monitored in the 105-210 nm region at an instrumental resolution of 0.1nm.

In the absorption c.s. of CS_2, vibrational progressions are observed in the 138-146, 158-163 and 180-183 nm regions. However, they are fairly irregular probably because of strong interactions among several upper states including 3d orbitals. Fig. 1 shows vibrational progressions in the absorption c.s. and fluorescence

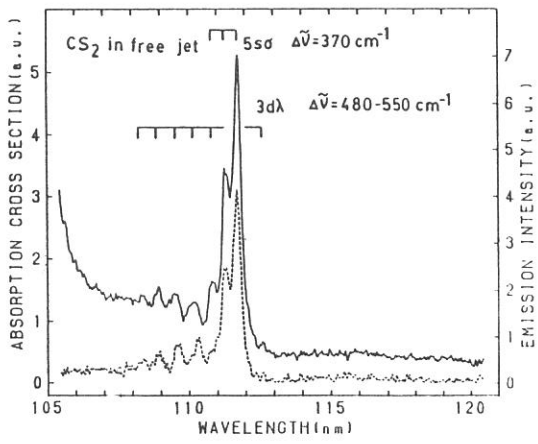

Fig.1.
Absorption c.s.(——) and fluorescnce e.s.(---) of CS_2 in a free jet.

e.s. in the 106-120 nm region. A strong absorption band at 111.7 nm and a band at 112.6 nm are assigned to the 5sσ and 3dλ Rydberg states, respectively, converging to the $CS_2^+(A^2\Pi)$ state[3]. The virational separation for the 111.7 nm band is found to be 370 cm^{-1}, while that for the 112.6 nm band is estimated to be 480-550 cm^{-1}. This result is inconsistent with the published data[3].

In the absorption c.s. of N_2O, we have not observed the structure in the 122-135 nm region.

The absorption spectra of N_2O in the 138-152 nm region, which is assigned to the $^1\Pi(bent) \leftarrow {}^1\Sigma^+$ transition, is known to show strong progressions. Its vibrational spacing is found to varies from 440 to 590 cm^{-1}. We consider that this irregularity results from strong interactions among the vibrational levels of two active modes.

Fig. 2. shows the fluorescence e.s. of jet-cooled N_2O in the 105-139 nm region. The emission below 118 nm consists of the $N_2(B^3\Pi_g - A^3\Sigma_u^+)$ and $NO(B^2\Pi - X^2\Pi)$ bands, while that above 120 nm is attributed to the NO(B-X) band. The $N_2(B)$ state is produced through the direct dissocation, $N_2O \rightarrow N_2(B)+O(^3P)$, while the NO(B) state is produced via secondary reactions such as $N_2O \rightarrow O(^1S)+N_2(X)$, $N_2O+O(^1S) \rightarrow NO(B)+NO(X)$[1]. Thus, the NO(B-X) emission is known to be suppressed by foreign gas as quenchers. The fluorescence e.s. in the 125-133 nm region at a stagnation pressure of 220 torr are very similar to that at 760 torr. This suggests that the precursor for the NO(B-X) band is highly quenched by N_2O in a free jet.

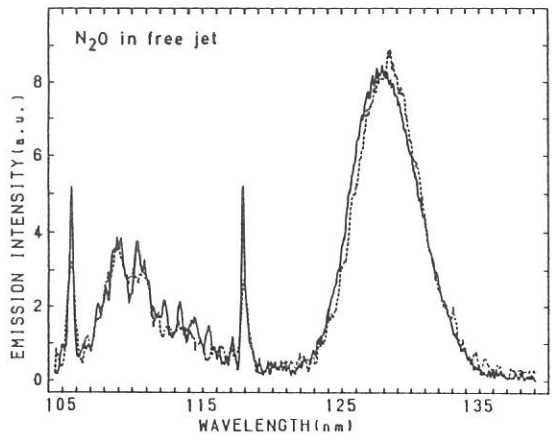

Fig. 2.
Fluorescence e.s. of jet-cooled N_2O normalized at 109 nm: the solid line, at a stagnation pressure of 760 torr and with a resolution of 0.2 nm; the broken line, 220 torr and 0.5 nm.

References

[1] L.C.Lee and M.Suto, J.Chem.Phys. 80, 4718(1984). [2] R.J.Hemley, D.G.Leopold, J.L.Roebber and V.Vaida, J.Chem.Phys. 79, 5219(1983).
[3] M.Larzilliere and N.Damany, Can.J.Phys. 56, 1150(1978).

Synchrotron Radiation Measurements of Appearance Potentials of $(H_2O)_2^+$, $(H_2O)_3^+$, $(H_2O)_2H^+$ and $(H_2O)_3H^+$

Haruo Shiromaru,[a] Hisanori Shinohara, Nobuaki Washida,[b] Hee-Soo Yoo,[c] and Katsumi Kimura

Institute for Molecular Science, Okazaki 444
(a Department of Chemistry, Tokyo Metropolitan University.)
(b The National Institute for Environmental Studies.)
(c Department of Chemistry, Chungbuk National University.)

The photoionization of water clusters gives rise to $[(H_2O)_n^+]^*_{vip} \rightarrow (H_2O)_{n-k}H^+ + OH + (k-1)H_2O$, where vip means the vertically ionized point. Ng et al.[1] have reported the appearance potentials (E_{ap}) for H_3O^+ and $(H_2O)_2^+$. For water clusters larger than the dimer, the parent ions $(H_2O)_n^+$ have not been observed. Recently, such unprotonated water cluster ions have been observed successfully by Shinohara et al.[2] in the photoionization of mixed clusters $Ar_m(H_2O)_n$ with ArI resonance lines. In the present work, we have used synchrotron radiation to measure appearance potentials of water cluster ions.

Photoionization experiments of water-Ar mixed clusters in supersonic jets were carried out with a molecular-beam apparatus on Beam Line BL2-B2.[3] Mass peaks which were observed here by a quadrupole mass spectrometer at different stagnation pressures at a wavelength of 85 nm are due to Ar_m^+ (m = 1-3), $(H_2O)_n^+$ (n = 1-6), $(H_2O)_nH^+$ (n = 1-6), $Ar_mH_2O^+$ (m = 1,2), $Ar_mH_3O^+$ (m = 1,2), $Ar(H_2O)_n^+$ (n = 1,2). Photoionization efficiency (PIE) curves were measured for several cluster ions.

The PIE curves of $(H_2O)_2^+$, $(H_2O)_3^+$, $(H_2O)_2H^+$ and $(H_2O)_3H^+$ obtained at the 7.0-atm stagnation pressure are shown in Fig. 1, together with some results of further signal accumulations performed near the onsets. The PIE curves of $(H_2O)_2^+$ and $(H_2O)_2H^+$, obtained at 4.0 atm at which the formation of water-Ar mixed cluster ions is negligibly small, are also shown in Fig. 1.

The E_{ap} values of $(H_2O)_2^+$, $(H_2O)_3^+$, $(H_2O)_2H^+$ and $(H_2O)_3H^+$ were determined to be 10.87 ± 0.06, 10.92 ± 0.04, 11.18 ± 0.02, respectively. From our results, we may deduce the following interesting tendencies. 1) The E_{ap} of $(H_2O)_2H^+$ is considerably lower than that of H_3O^+, whereas the E_{ap} of $(H_2O)_3H^+$ is only slightly lower than that of $(H_2O)_2H^+$. 2) The E_{ap} of $(H_2O)_3^+$ is almost the same as that $(H_2O)_2^+$. 3) The E_{ap} of $(H_2O)_3^+$ is lower by 0.26 eV than that of $(H_2O)_2H^+$. 4) The PIE curve of $(H_2O)_2H^+$ does not depend on the stagnation pressure.

For water clusters the direct photoionization process is expected to be dominant, since the PIE curve of H_2O^+ shows no distinct autoionization structure. In the water dimer, its E_{ap} is much higher than the corresponding adiabatic ionization energy. The E_{ap} of H_3O^+ corresponds most likely to the adiabatic energy of the formation of H_3O^+ from $(H_2O)_2$.

The $(H_2O)_3^+$ ion is not observed from the water trimer, because of the Franck-Condon restriction. The E_{ap} of $(H_2O)_2H^+$ is

more or less higher than its adiabatic energy. At the high stagnation pressure, however, $(H_2O)_3^+$ can be observed due to the process $Ar_m(H_2O)_n + h \rightarrow (H_2O)_p^+ + mAr + e^-$. This process may be explained in terms of two effects: (a) the perturbation of the potential curve by the attachment of Ar atoms, and (b) the internal excess energy dissipation by the evaporation of the Ar atoms as translational energies.

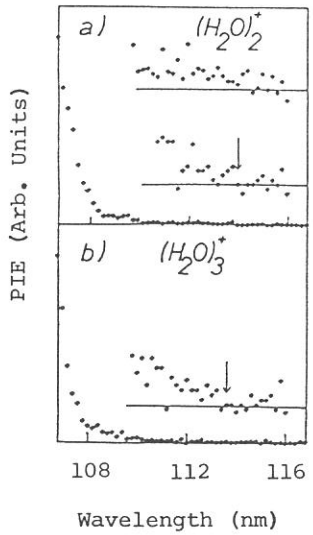

Fig. 1. The PIE curves for produ-producing cluster ions at a stag-nation pressure of 7.0 atm. The results at a lower stagnation pressure (4.0 atm are also shown on the top of (a) and (b).

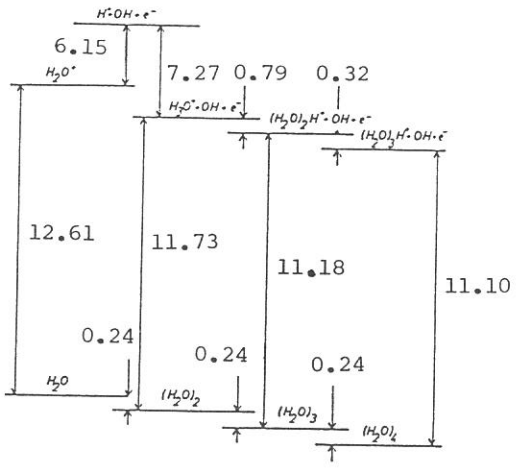

Fig. 2. Energy level diagram of water cluster and pronotnated ions, showing proton solvation energies, in eV units.

$E_{ap}[(H_2O)_3^+]$ is lower than $E_{ap}[(H_2O)_2H^+]$ by 0.26 eV, suggesting that the Franck-Condon region covers a smaller part of the potential minimum for the water trimer ion compared to that for the dimer ion. This is one of the reasons for the small appearance potential difference between $(H_2O)_2^+$ and $(H_2O)_3^+$.

Since the A_p of the protonated ion $(H_2O)_nH^+$ may be regarded as the adiabatic energy, thermochemical properties of the water clusters can be derived from the present results. A schematic energy level diagram relevant to the present work is shown in Fig. 2.

1) C. Y. Ng, D. J. Trevor, P. W. Tiedemann, S. T. Ceyer, P. L. Kronebusch, B. H. Mahan and Y. T. Lee, J. Chem. Phys., **67**, 4235 (1977).

2) H. Shinohara, N. Nishi and N. Washida, J. Chem. Phys. **84** 5561 (1982).

3) Shiromaru, Y. Achiba, K. Kimura and Y. T. Lee, J. Phys.

EVAPORATION PROCESSES OF WATER CLUSTER IONS AND CO_2-WATER MIXED CLUSTER IONS PRODUCED BY SYNCHROTRON RADIATION

Haruo SHIROMARU,[a] Hideyuki SUZUKI,[b] Masahiro KAWASAKI, Hiroyasu SATO,[b] Shin-ichi NAGAOKA and Katsumi KIMURA

Institute for Molecular Science, Okazaki 444
(a Department of Chemistry, Tokyo Metropolitan Univ.
(b Department of Chemistry, Mie Univ.)

In the event of photoionization of water clusters, as is well known, various protonated ions are mainly produced.

$$(H_2O)_n + h\nu \rightarrow (H_2O)_{n-k-1}H^+ + k(H_2O) + OH + e^- \quad (1)$$

For CO_2- water mixed clusters, the ionization leaving unprotonated water cluster ions also take place.

$$(CO_2)_m(H_2O)_n + h\nu \rightarrow (H_2O)_{n-k}^+ + k(H_2O) + m(CO_2) \quad (2)$$

In these reactions, evaporation processes of $k(H_2O)$ and/or $m(CO_2)$ play an important role for the dissipation of the internal energy.

In the present work, the evaporation processes involved in the reactions (1) and (2) were studied by measuring photoionization efficiency (PIE) curves of the water cluster ions. The effect of H_2O evaporation was examined by comparing the PIE curves obtained with various stagnation pressures (Ps) of Ar, because the size distribution of neutral water clusters largely depends on Ps. Since large size water clusters were hardly produced for low Ps, the PIE curve shown in 1a should be purely due to the ionization of $(H_2O)_2$. The contribution of larger cluster is important for higher Ps and is observed as the extra signals in shorter wavelength region of Fig. 1b,c,d.

The PIE curves of water cluster ions produced from the CO_2 seeded H_2O are shown in Fig. 2. The broad peaks at 76 nm and 88 nm are assigned to the ionization of the CO_2 site of the mixed

cluster $(CO_2)_m(H_2O)_n$. Therefore, the intra-cluster charge transfer reactions before CO_2 evaporation should play an important role for producing water cluster ions, especially for unprotonated water cluster ions (reaction 3).

$$(CO_2)_m(H_2O)_n + h\nu \rightarrow [(CO_2)_m^+ : (H_2O)_n]$$
$$\rightarrow (H_2O)_{n-k}^+ + m(CO_2) + \cdots \quad (3)$$
$$\rightarrow (H_2O)_{n-k-1}H^+ + m(CO_2) + \cdots \quad (4)$$

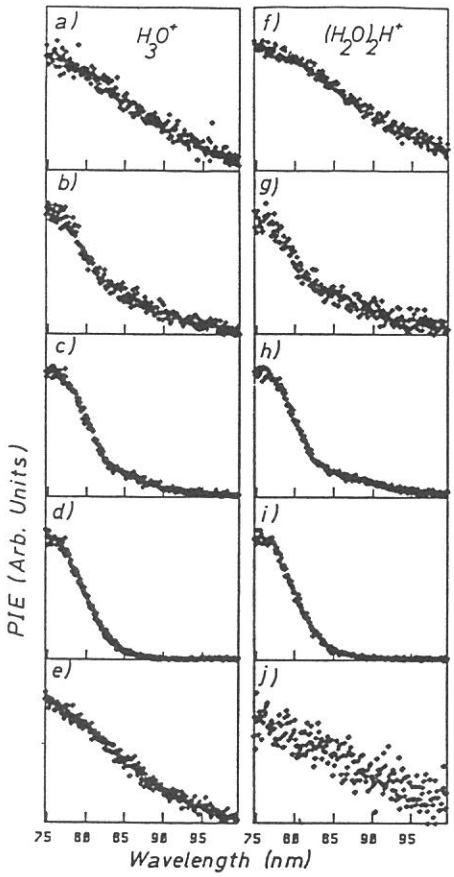

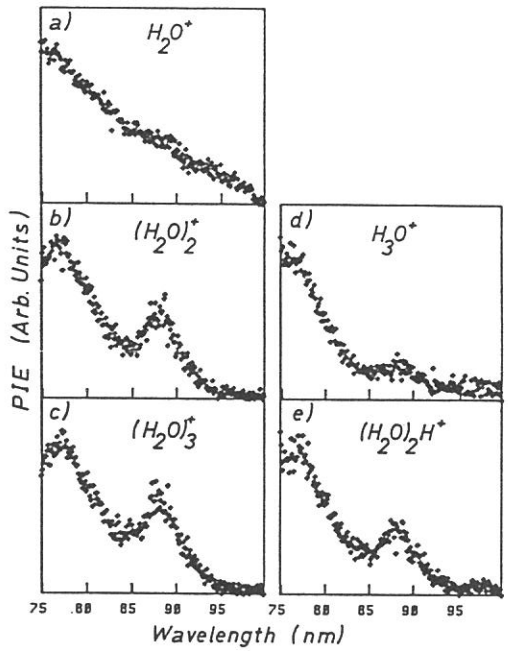

fig.2 PIE curves measured with 4.0 atm of CO_2.

Fig. 1. The PIE curves measured at various Ps.
Large size clusters are not produced by He seeding.
Ps = 0.4 atm (a, f); 2.2 atm (b, g); 3.5 atm (c, h);
7.8 atm (d, i) of Ar. 7.8 atm of He (e, j).

INTRAMOLECULE-INTERMOLECULAR AUTOIONIZATION WITHIN A VAN DER WAALS MOLECULE

M.Ukai

Photon Factory, National Laboratory for High Energy Physics,
Tsukuba-shi, Ibaraki 305

T.Kamosaki, K.Kameta, K.Shinsaka, and Y.Hatano

Department of Chemistry, Tokyo Institute of Technology,
Meguro-ku, Tokyo 152

S.Nagaoka and K.Kimura

Institute of Molecular Science,
Myodaiji, Okazaki-shi, Aichi 444

Penning ionization processes by optically allowed rare gas atoms, being one of the basically important chemical reactions, have not been studied very extensively because of experimental difficulties owing to the short lifetimes of the atoms. Very recently, our group has reported the studies for some fundamental cases.[1)]

Synchrotron radiation (SR) is one of the most powerful tools to study atomic and molecular photoionization processes in the VUV region. It has been pointed out that SR is also very advantageous to investigate intermolecular processes. Up until present, however, only a few studies have been reported owing to lower intensity of SR in comparison with the conventional excitation sources.

We would like to propose here an experimental investigation on Penning ionization including optically allowed rare gas atoms. The rare gas site of a van der Waals molecule, such as NeM, produced in a supersonic free expansion would be excited by a slightly shifted resonance radiation of SR up to the resonance state of $Ne(3s^1P_1)$.[2,3)] Because the excitation energy of Ne resonance state is larger than the ionization potential of atoms and molecules M, the molecular excited state of $(NeM)^*$ will undergo autoionization to produce Ne^++M or NeM^+. Figure 1 shows the preliminary photoionization efficiency curve for $NeAr^+$ around 73.7nm[2)] obtained at BL-2B2 of UVSOR, IMS,

by using a quadupole mass spectrometer. The peak around 73.7nm corresponds to the autoionization structure due to intermolecular Penning ionization. By analyzing the line shape of the spectrum, it would be possible to extract the autoionization width for Penning ionization or the information on the interaction potential for Ne^*-Ar. For cases M is a molecule, we can obtain partitioning probability of the resonance energy into various ionic fragments if transferred from complex partner, which might offer not only coplementary information on molecular photoionization by NeI but also new information on specific fragmentation from another site.

1)M.Ukai et al, J.Chem.Phys.,84, 3199(1986);84,5575(1986);88(in press).
2)P.M.Dehmer & S.T.Pratt,"*Photophysics and Photochemistry in the Vaccum Ultraviolet*", NATO ASI Series C ; Vol 142 (Reidel, Dordrecht,1985) p467.
3)B.Kamke et al,J.Chem.Phys.,86, 2525(1987).

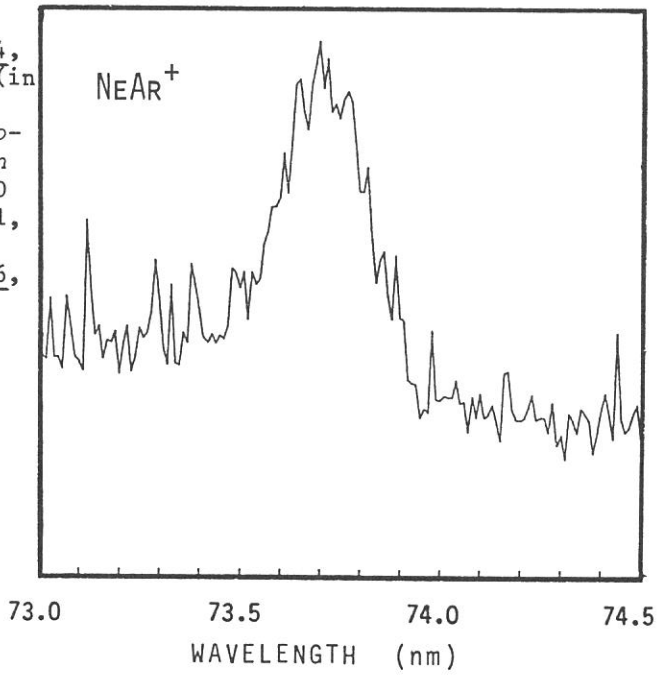

Figure 1. Photoionization efficiency curve for $NeAr^+$

BINARY CLUSTER OF OIL AND WATER: ETHYLENE - WATER

Shin-ichi NAGAOKA, Haruo SHIROMARU, Takato HIRAYAMA and Katsumi KIMURA

Institute for Molecular Science, Okazaki 444, Japan

Oil and water will not blend. It is interesting to study the properties of the interface between oil and water. The cluster can be regarded as a model of the interface. Hence, it seems worthwhile to make a detailed investigation of oil-water binary clusters in order to elucidate the properties of the interface between oil and water. Photoionization measurements for ethylene-water binary clusters were performed by use of synchrotron radiation from the beam line BL2B2.

Figure 1 shows the photoionization efficiency curves for $(C_2H_4)(H_2O)_n^+$ (n=1-3) near the threshold. Addition of H_2O to $(C_2H_4)(H_2O)$ does not affect the appearance energy of the corresponding ion. If the structure of $(C_2H_4)(H_2O)_n$ (n=2,3) is as follows, $...H_2O...C_2H_2...H_2O(...H_2O)$, or if an electron delocalized over the cluster is ejected in the photoionization, the appearance energies of $(C_2H_4)(H_2O)_n^+$ (n=2,3) are considered to be different from that of $(C_2H_4)(H_2O)^+$. Thus, one may suppose that the structure of $(C_2H_4)(H_2O)_n$ (n=2,3) is as follows, $C_2H_4...H_2O...H_2O(...H_2O)$, and that in the photoionization of $(C_2H_4)(H_2O)_n$ (n=1-3), an electron localized at C_2H_4 is ejected.

Ab initio SCF calculations of $(C_2H_4)(H_2O)$ were carried out with Gaussian 82 programs using the 4-31G double-zeta basis set. The result of the geometry optimization is shown in Fig. 2. The dissociation energy of the optimized cluster was obtained to be

1.6 kcal/mol. This value is larger than the dissociation energy of $(C_2H_4)_2$ (0.5 kcal/mol), and is smaller than that of $(H_2O)_2$ (5.5 kcal/mol). At the interface between oil and water, H_2O molecules form strong hydrogen-bonds among themselves. From the calculation results described above, it seems that oil is more likely to link to water than to gather in a block. However, since water is closely united, oil cannot get into water phase. Oil can form the pseud-hydrogen-bond with water only at the interface.

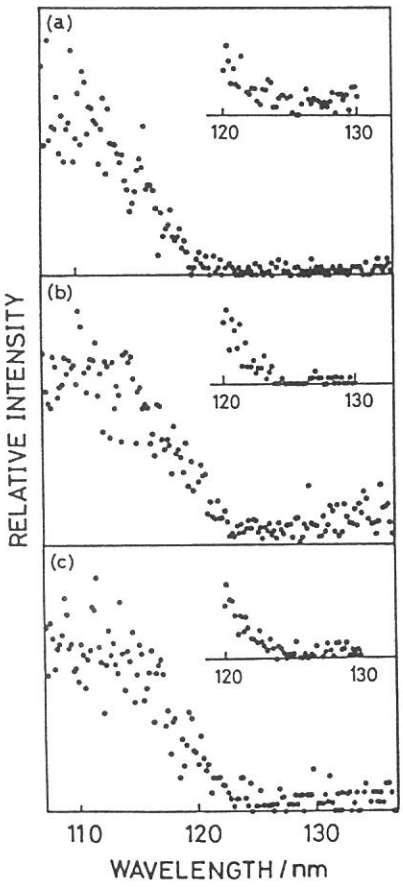

← Fig. 1. Photoionization efficiency curves for $(C_2H_4)(H_2O)$ (a), $(C_2H_4)(H_2O)_2$ (b) and $(C_2H_4)(H_2O)_3$ (c) near the threshold.

↓ Fig. 2. Optimized geometry, in A and degree, $(C_2H_4)(H_2O)$.

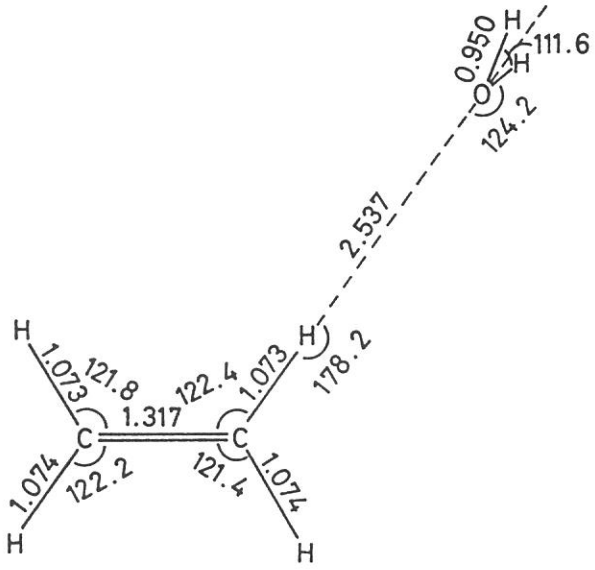

INVESTIGATION OF FRAGMENTATION PROCESSES FOLLOWING CORE PHOTOEXCITATION OF TETRAMETHYLGALLIUM IN THE VAPOR PHASE

Shin-ichi NAGAOKA, Shinzo SUZUKI, Takashi IMAMURA and Inosuke KOYANO

Institute for Molecular Science, Myodaiji, Okazaki 444

In recent years, dynamic processes following core level excitation in molecules have been a topic of much interest. We have investigated the dynamic processes of organometallic molecules with group II-V elements following the core level excitation by using the threshold electron – photoion coincidence (TEPICO) method.[1] Here, we report the fragmentation of trimethylgallium (TMGA). The experiments were performed using the TEPSICO-II apparatus[2] installed in BL3B beam line of UVSOR.

Figure 1 shows the threshold electron spectrum of TMGA. Sharp bands seen at 48.3 and 60.9 nm are assigned to the photoionization from the Ga 3d core level and the Ga 3d→σ* transition, respectively. It is found that a threshold electron is ejected by way of autoionization following the Ga 3d→σ* transition. Figure 2 shows the photoionization efficiency curves for fragment ions from TMGA. The peak due to the Ga 3d→σ* transition is seen in those curves, and is the highest in the Ga^+ curve. Figure 3 shows an example of the TEPICO spectrum. It is seen that sufficiently high signal-to-noise ratio is attained with reasonable data collecting time. Branching ratio of TMGA was determined by use of TEPICO, and are given in Fig. 4. From these results, it is considered that the Ga^+ ion is predominantly produced following Ga 3d core photoexcitation, and that $GaCH_3^+$ ion is produced following both 3d excitation and valence photoionization.

References

1. S. Nagaoka, S. Suzuki and I.Koyano, Phys. Rev. Lett., 58, 1524 (1987); Nucl. Instrum. Methods, in press.
2. S. Suzuki, S. Nagaoka, I. Koyano, K. Tanaka and T. Kato, Z. Phys., D4, 111 (1986).

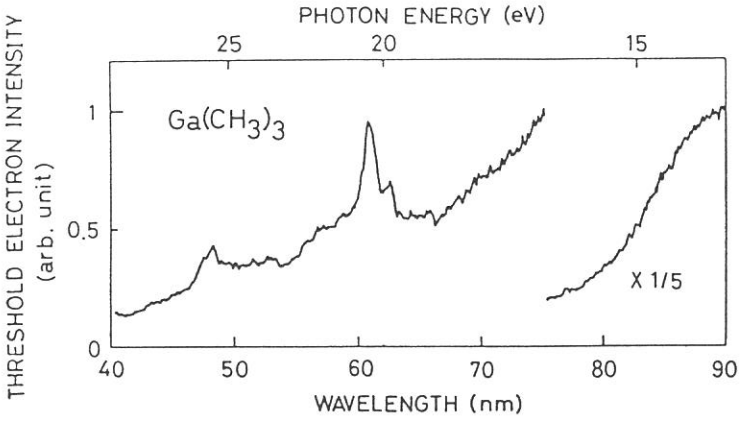

Fig. 1. Threshold electron spectrum of TMGA

Fig. 3. Time-of-flight TEPICO spectrum of the Ga^+ ion taken by excitation at 48.3 nm. Data collection time is 55 min. ⟶

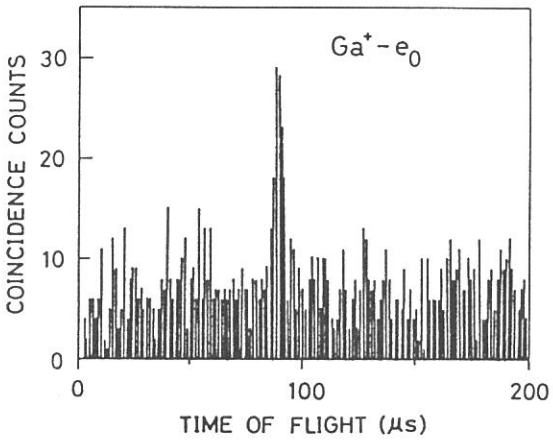

↓ Fig. 2. Photoionization efficiency curves of TMGA.

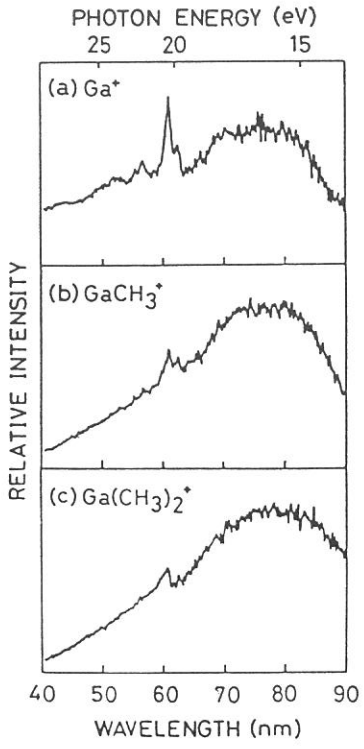

Fig. 4. Branching ratio

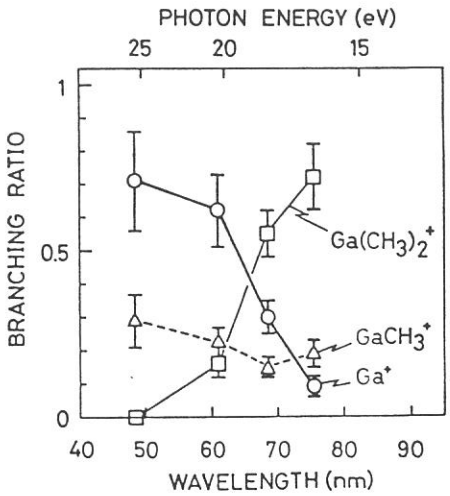

STUDIES OF THE STATE SELECTED ION-MOLECULE REACTIONS $Ne^+(^2P_{3/2}, ^2P_{1/2})$ + OCS USING TEPSICO-II APPARATUS

Shinzo Suzuki, Takashi Imamura and Inosuke Koyano

Institute for Molecular Science, Myodaiji, Okazaki, 444

Toward the study of state-selected ion-molecule reactions, the TEPSICO-II apparatus[1] has been installed at the beam line BL3B of UVSOR. This apparatus is suitable for the study of reactions of ions whose ionizaton thresholds lie in the far VUV region down to 30 nm. Ion-molecule reactions of Ne^+ are favorable candidates for such a study because its first ionization thresholds ($^2P_{3/2}$ and $^2P_{1/2}$) lie in the above-mentioned wavelength region.

Here we report a preliminary result on the ion-molecule reaction Ne^+ + OCS, obtained using the TEPSICO-II apparatus but without selecting reactant states. For this reaction system, three reaction channels,

$$Ne^+ + OCS \rightarrow CO^+ + S + Ne \quad (1)$$
$$\rightarrow S^+ + CO + Ne \quad (2)$$
$$\rightarrow CS^+ + O + Ne \quad (3)$$

have been reported using a selected ion flow tube (SIFT) apparatus.[2]

Figs. 1 and 2 show the threshold electron spectrum and the photoionization efficiency curve of Ne, respectively, in the wavelength region 55.5-58.0 nm. The threshold electron spectrum clearly shows two peaks corresponding to the formation of the two spin-orbit states, $^2P_{1/2}$ and $^2P_{3/2}$, of Ne^+, although their resolution is not complete. Fig. 3 shows the efficiency curve for the reaction product CO^+, which indicates that reaction (1) opens above the first ionization threshold of Ne. The efficiency curve for S^+ (reaction (2)) was also obtained but that for CS^+ (reaction(3)) was not obtained because of its extremely weak intensity.

These results demonstrate the feasibility of the state-selected studies of the Ne^+ reactions using coincidence measurements. However, such experiments need further refinement of the resolution of the threshold electron analyzer and the increase in the intensity of the primary ions (or monochromatized photons), which are now under way.

REFERENCES

1) I. Koyano, K. Tanaka, T. Kato, and E. Ishiguro, UVSOR Activity Report 1984/85, p.31.

2) A. B. Rakshit and N. D. Twiddy, Chem. Phys. Lett., 60, 400 (1979).

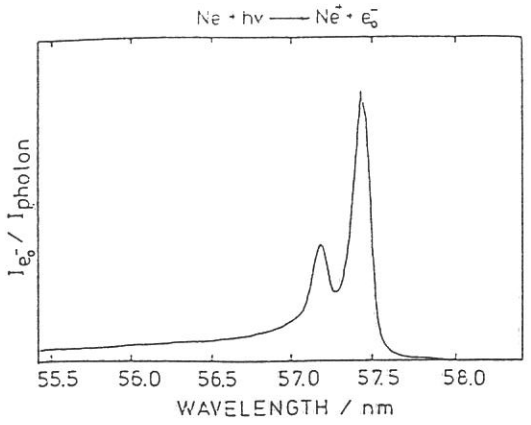

Fig. 1 Threshold electron spectrum of Ne

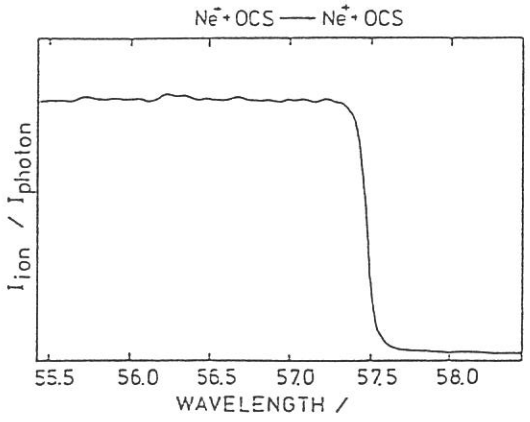

Fig. 2 Photoionization efficiency curve of Ne

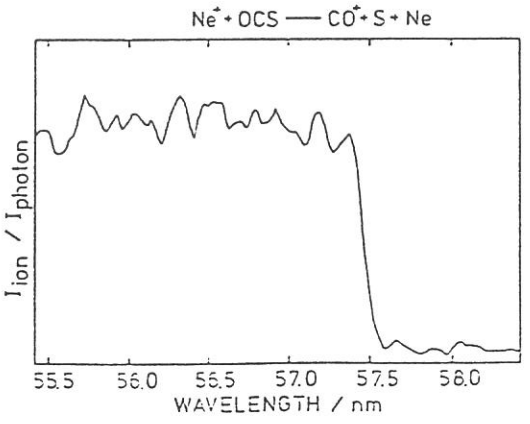

Fig. 3 Efficiency curve for the reaction product CO^+

Reflection Spectra of $CuInSe_2$ from 2 to 100 eV

Kenichi TAKARABE

Department of Natural Science, Faculty of Science, Okayama University of Science, Ridai-cho, Okayama 700

We report reflectivity up to 100 eV of the chalcopyrite semiconductor $CuInSe_2$ using synchrotron radiation for the first time. P-like partial density of states in the conduction band are identified from the sharp structures at 18 to 22 eV. These structures originate due to the transitions from the In $4d_{5/2}$ core level to the conduction band.

The chalcopyrite semiconductor $CuInSe_2$ is a promising material for solar cells with excellent reliability and high power-conversion efficiency. For further cell improvements research has been started to gain a fundamental knowledge of this material. Figure 1 shows the reflection spectra of $CuInSe_2$ in the photon energy from 2 to 100 eV measured by synchrotron radiation source(SR). The reflection spectra is classified into three groups. The reflection spectra from 2 to 10 eV is originated from the transitions from valence to conduction band(CB). At about 20 eV the reflection feature corresponds to the transitions from In 4d core level to CB. Also, at about 55 eV the structures corresponding to the transitions from Se 3d core level to the CB are observed. For further consideration on the features around 20 eV the blowup of reflectivity is shown in Fig. 2. According to UPS studies the In $4d_{5/2}$ core level is 17.0 eV below the top of valence band. Thus there is no doubt that the features in the reflectivity are the In 4d core reflectivity. Optical dipole transitions originating from d states are only allowed to terminate at p-like states. Each three peaks thus reveals a partial p-like density of states in the conduction band. Observed each peaks is assigned to S_1 to S_3. The locations of energies are determined from a numerical derivative of spectra.The temperature effect on each peak differs from each others. Decreasing temperature S_1 peak shifts to a higher energy location accompanied by a slight sharpening. S_2 peak shows only a slight sharpening but no energy shifts. S_3 peak shows a large sharpening without energy shifts. These temperature variations of spectral features are understood as electron transfer spectra in local atomic arrangements in $CuInSe_2$ shown in Fig. 3. In a general sense, for the case of intratomic transition of electron we may expect no energy shift and only sharpening of lifetime broadening with decreasing temperature. The S_2 structure realizes this situation, so the structure corresponds to the transition on In atom from 4d to 5p state. For the interatomic transition of electron we may expect a blue shift of photon energy due to shortening interatomic distance and sharpening of spectral shape due to depressing of interatomic stretching vibrations with decreasing temperature. The S_1 structure realizes this feature well, so the S_1 structure originates from the interatomic transition from In 4d to Se 5p state. The copper and indium atoms are coupled with the bending force. Due to a weaker force

constant than the force constant of stretching vibration, the degree of spectral feature sharpening with decreasing temperature is larger than with the streching vibration. Also the shrinkage of interatomic distance is smaller than the distance between selenium and indium. The S_3 structure well reproduces this anticipation, so the transition occurs from In 4d to Cu 4p state. The identification including the spin-orbit splitting energy of In 4d core electrons is excluded, because this splitting energy, 0.8 eV, is less than the energy difference between observed reflection peaks(S_1 to S_3) in Fig. 2. Next, we infer taht the weak inflection at about 17.4 eV is the transition from In 4d to the CB minimum.

This work was supported by the Joint Studies Program(1985-1986) of the Institute for Molecular Science.

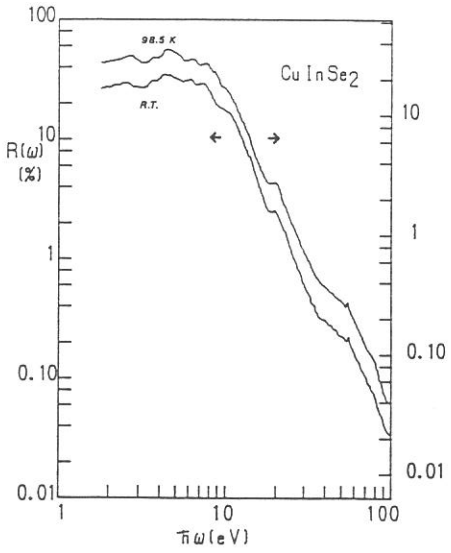

Fig. 1. Reflection spectra on the (112) face of a $CuInSe_2$ single crystal for room temperature and 98.5 K.

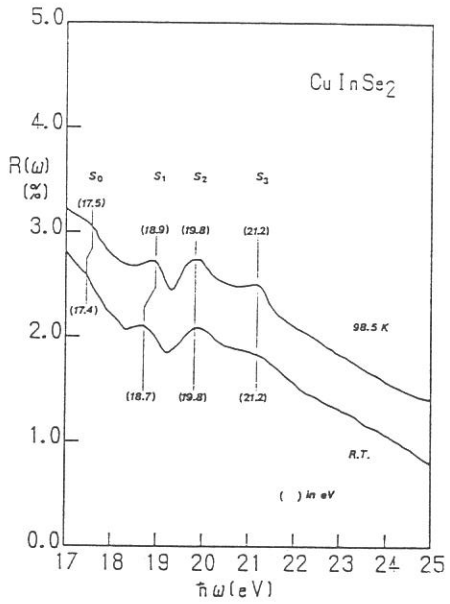

Fig. 2. A blowup of Fig. 2 from 17 to 25 eV. Observed features are designated as S_1 to S_3.

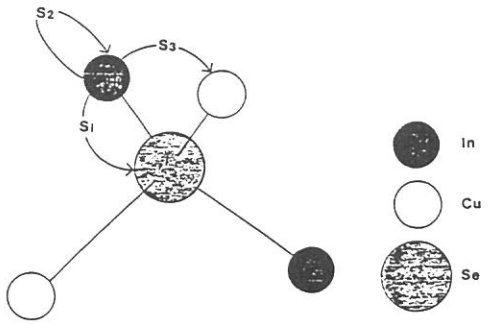

Fig. 3. The local atomic arrangement in $CuInSe_2$.

OPTICAL ABSORPTION SPECTRA OF PbI_2 SINGLE CRYSTALS

Tetsusuke HAYASHI, Koichi TOYODA* and Minoru ITOH**

College of General Education, Kyoto University, Kyoto 606

*Department of Physics, Osaka Dental University, Hirakata, Osaka 573

**Institute of Physics, Faculty of Engineering, Shinshu University, Nagano 380

Absorption spectra of PbI_2 single crystals have been investigated between 2 and 100eV. The spectra were obtained from Kramers-Kronig analysis of reflectivity data measured at 5K by using a plane grating monochromator at BL6A. The incident light was near normal to the basal plane of the crystal.

Figure 1 shows absorption spectra form 2 to 12eV for crystals having 2H and 4H polytypes. The spectrum of the 2H crystal is almost similar to that reported already.[1] According to band structure calculation by Schlüter et al.,[2] the peaks 1, 2 and 3 are assigned to excitonic transitions at A-point of the Brillouin zone from Pb^{++} 6s-like valence band to 6p-like conduction band, and the peaks 4, 5 and 6 are to those from I^- 5p-like valence band also at A-point. These peaks as well as those labeled 9 to 11 are observed in 4H crystal at almost the same energies, whereas some peaks or humps have shifts of about 0.2 to 0.5eV from the 2H spectrum as denoted by arrows. Change of the polytype from 2H to 4H induces a folding of bands along a direction of c-axis of the Brillouin zone. Then a transition at A-point in 2H structure is transferred to that at Γ-point in 4H structure, and similarly the one at L-point to that at M-point. Band structure calculations for the similar layered compounds have suggested that the change in the transition energy due to the folding of the band is negligible at the zone center, while a noticeable change appears at the zone boundary.[3] It is, therefore, likely that the structures different among the two spectra are due to transitions at the zone boundary, at L or M-points.

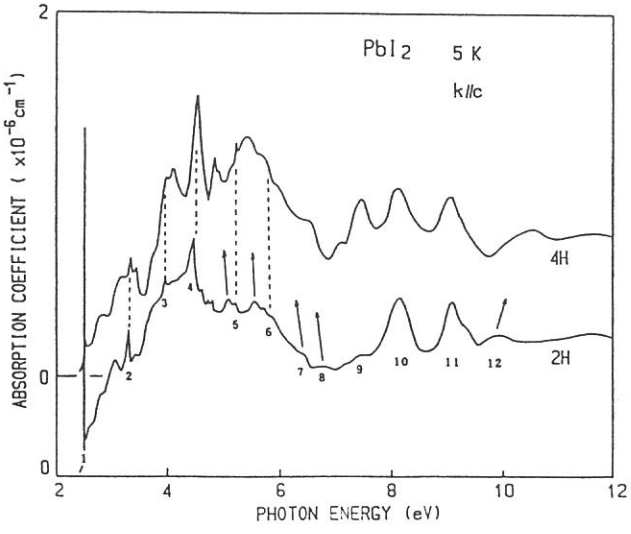

Fig. 1

Sharp absorption structures appear between 18 and 24eV as shown in Fig.2. These have been attributed to transitions from Pb^{++} 5d core states.[1] Some of the energy levels of a free Pb^{++} ion are shown in the figure for a comparison, which have been shifted 0.6eV from the true values so as to fit the $^1P_1$ level to the prominent peak. The fairly well correspondence suggests that the observed structures are due to highly localized excitations on Pb^{++} ions from 5d core to 6p levels. According to the photoelectron spectra reported by Azoulay et al.,[4] the Pb^{++} $5d_{3/2}$ and $5d_{5/2}$ levels are located at 20.4eV and 17.8eV below the top of the valence band. The transition from Pb^{++} $5d_{5/2}$ to 6p in a free ion is optically forbidden, but a small hump is seen at 19.5eV in the figure. As the energy difference from the $^1P_1$ peak is very close to the spin-orbit splitting energy (dashed line), the hump may be assigned to the Pb^{++} $5d_{5/2}$ core exciton. The estimated binding energies are ~0.6eV and 0.9eV for Pb^{++} $5d_{3/2}$ and $5d_{5/2}$ core excitons, respectively.

Figure 3 shows the absorption due to transitions from I^- 4d core states. Addition of the band gap energy to the photoelectron emission data ($4d_{3/2}$ -- 49.3eV and $4d_{5/2}$ -- 47.7eV)[4] gives the exact coincidence with the observed peaks having the splitting of 1.6eV as indicated in the figure. Therefore, the spectrum is explained as the transitions from I^- 4d core levels to the conduction band. The paired structures of 1.4eV shown in the figure correspond to the splitting of the conduction band (two A_4^-).

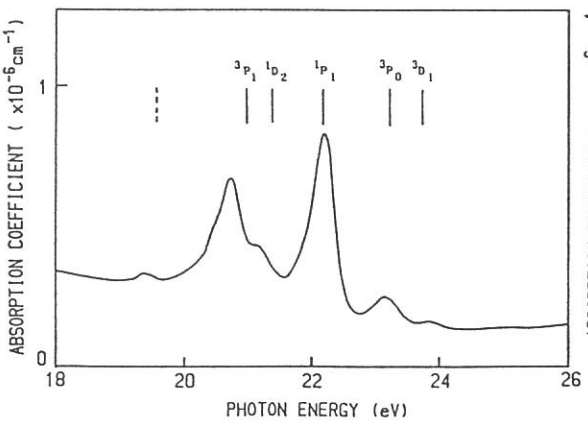

Fig. 2

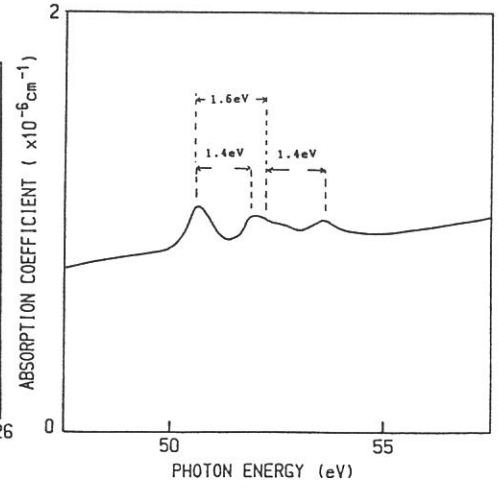

Fig. 3

1) J.Beaumont, A.Bourdillon and J.Bordas: J. Phys. C:10 (1977) 761.

2) L.Ch.Schlüter and M.Schlüter: Phys. Rev. B9 (1974) 1652.

3) R.Coehoorn, G.Sawatzky, C.Haas and R.de Groot: Phys. Rev. B31 (1985) 6739.

4) J.Azoulay and L.Ley: Solid State Commun. 22 (1977) 557.

Ni $L_{2,3}$ PHOTOELECTRIC YIELD SPECTRA OF SOME Ni(II) COORDINATION COMPOUNDS

Masayoshi OBASHI, Tokuo MATSUKAWA, Seiko KOMORITA* and Akira TAKEUCHI*

Department of Physics, College of General Education, Osaka University
Machikaneyama, Toyonaka 560
*Department of Chemistry, College of General Education, Osaka University
Machikaneyama, Toyonaka 560

The photoelectric yield emitted by a sample is directly proportional to its absorption coefficient. Therefore,the Ni $L_{2,3}$ yield spectra of some nickel (II) coordination compounds with different coordinations were measured at BL-7A in order to study the influences of the chemical bonding and immediate surroundings of the central nickel ion on these Ni $L_{2,3}$ absorption spectra.

Samples studied here were as follows;(a)tris(ethylenediamine)nickel(II)chloride dihydrates ($[Ni(en)_3]Cl_2 \cdot 2H_2O$),(b) the brown room temperature phase of bis[N-(3-methoxysalicylidene)iso-propylaminato]nickel(II) ($[Ni(3\text{-}MeO\text{-}sal\text{-}i\text{-}Pr)_2]$),(c) the green room temperature phase of bis[N-(3-methoxysalicylidene)normal-propylaminato]nickel(II) ($[Ni(3\text{-}MeO\text{-}sal\text{-}n\text{-}Pr)_2]$) and (d)potassium tetracyano nickelate (II)monohydrate ($K_2[Ni(CN)_4] \cdot H_2O$). All yield spectra were measured in fine powder form by using a high-resolution vacuum two-crystal monochromator with beryl crystals.

Figure 1 shows the Ni $L_{2,3}$ absorption spectra of the present Ni(II)coordination compounds. Table 1 shows the electron configurations and coordinations of the nickel ion in the same compounds.

All Ni $L_{2,3}$ absorption spectra ($Ni2p_{1/2,3/2}-Ni3d$ transitions) consist of L_2(~870 eV) and L_3(~850 eV) edge structures split due to the spin-orbit interaction in the $2p_{1/2}$ and $2p_{3/2}$ hole respectively which are further split by other interactions.This is a so-called multiplet splitting of the absorption spectrum. Structures in the spectra are designated by capital letters A through E. The structures A of all the compounds, and the structures B and D of $[Ni(3\text{-}MeO\text{-}sal\text{-}n\text{-}Pr)_2]$ and $K_2[Ni(CN)_4] \cdot H_2O$ are an extremely narrow absorption line.

According to chemistry,the covalency of $[Ni(3\text{-}MeO\text{-}sal\text{-}i\text{-}Pr)_2]$,$[Ni(en)_3]Cl_2 \cdot 2H_2O$,$[Ni(3\text{-}MeO\text{-}sal\text{-}n\text{-}Pr)_2]$ and $K_2[Ni(CN)_4] \cdot H_2O$ increases in the listed order. It is noticeable that the energy positions of structures A and D of the above four compounds shift toward higher energies in the same order respectively.

The similarity of $[Ni(en)_3]Cl_2 \cdot 2H_2O$ and $[Ni(3\text{-MeO-sal-i-Pr})_2]$ spectra may be due to the similar crystal fields of the respective octahedral and tetrahedral coordinations. Also the similarity of $[Ni(3\text{-MeO-sal-n-Pr})_2]$ and $K_2[Ni(CN)_4] \cdot H_2O$ spectra may be due to the same coordinations (square plannar).

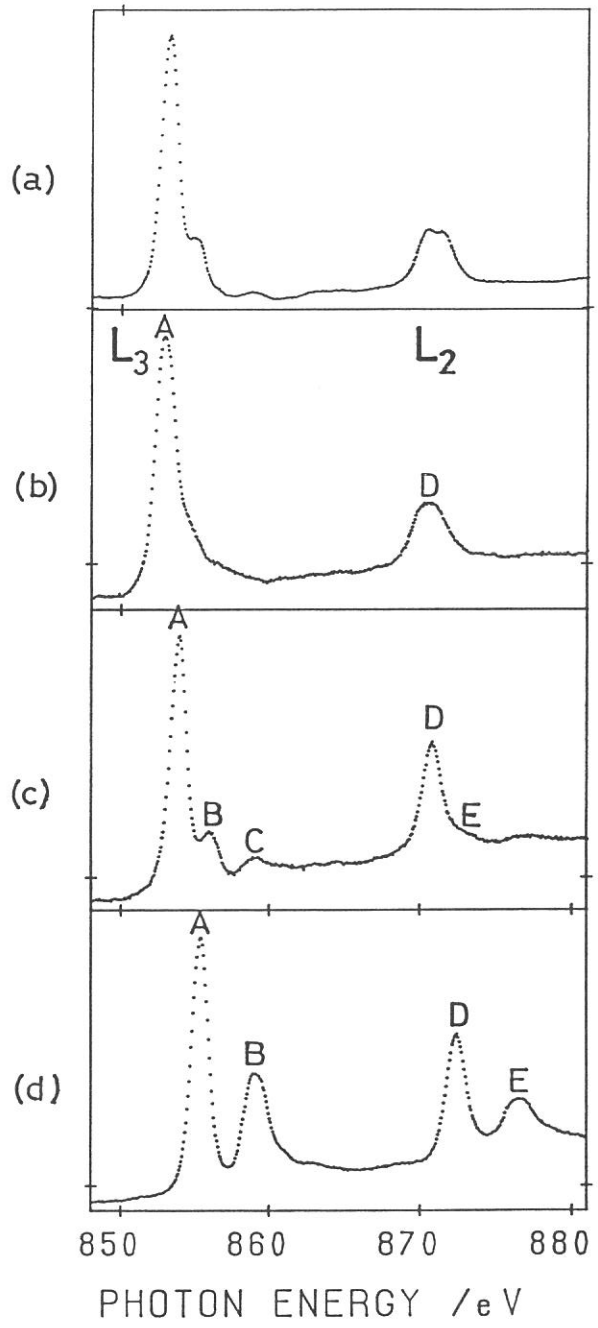

Fig.1. Ni $L_{2,3}$ absorption spectra of Ni(II) coordination compounds.

Table 1. Electron configurations and coordinations of nickel ion.

(a) $[Ni(en)_3]Cl_2 \cdot 2H_2O$

d^8, high spin type
octahedral

(b) $[Ni(3\text{-MeO-sal-i-Pr})_2]$

d^8, high spin type
tetrahedral

(c) $[Ni(3\text{-MeO-sal-n-Pr})_2]$

d^8, low spin type
square plannar

(d) $K_2[Ni(CN)_4] \cdot H_2O$

d^8, low spin type
square plannar

Na K-XANES and EXAFS Studies in $K_{1-x}Na_xCl$

Takatoshi MURATA, Tokuo MATSUKAWA*, Shunichi NAO-E**,

Department of Physics, Kyoto University of Education, Fushimi-ku, Kyoto 612
*Department of Physics, College of General Education, Osaka University, Machikaneyama, Toyonaka 560
**Department of Physics, College of General Education, Kanazawa University, Kanazawa 920

K-edge absorption specta of Na in $K_{1-x}Na_xCl$ were measured at BL-7A soft x-ray beam line by using double crystal monochromator[1] with flat beryls as monochromator crystals. Samples were prepared in the form of ingots and were evaporated in situ onto polyester film of thickness of about 0.5μm. Measurements were made at room temperature and at about 35K.

Figure 1 shows the Na K-edge absorption spectra of pure NaCl at room temperature (dashed curve) and at about 35K (solid curve). In Fig. 2 are shown XANES spectra of Na K-edge of the solid solutions at about 35K. All the spectra are normalized at the hieght of the first peak at 1076.6eV. The characteristic behavior of the small structure A strongly suggests that this is attributed to the forbidden transition. A reasonable assignment of the structure A may be the "forbidden Γ_1 exciton", which has been observed in Li K-absorption specturm in LiF[2]. The peaks B and D are very prominent and persistent in all the spectra. The peak B can be assigned as exciton associated with the transition to the conduction state with p-character. The origin of the peak D is not clear at the moment, but might be assigned as a structure due to multiple scattering of the excited electron[3].

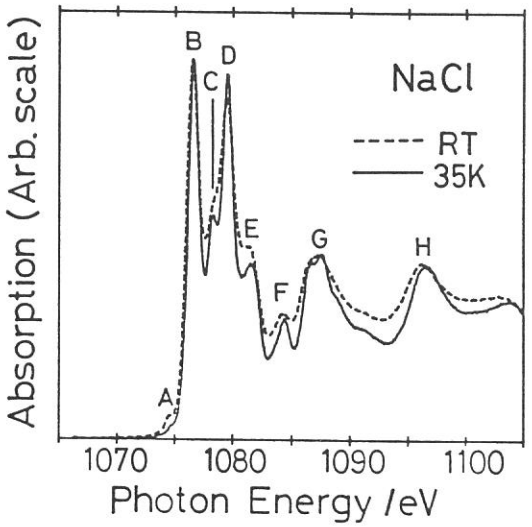

Fig. 1 Na K-edge spectra of NaCl at room temperature and at about 35K.

The magnitudes of the Fourier transforms of k^3 weighted EXAFS for each spectrum are shown in Fig. 3. The first shell distance of a Na^+ ion is not sensitive to the concentration of NaCl. This means that Cl^- ions around a Na^+ ion are coordinated conserving the inter-ionc distance of the pure NaCl in KCl matrix.

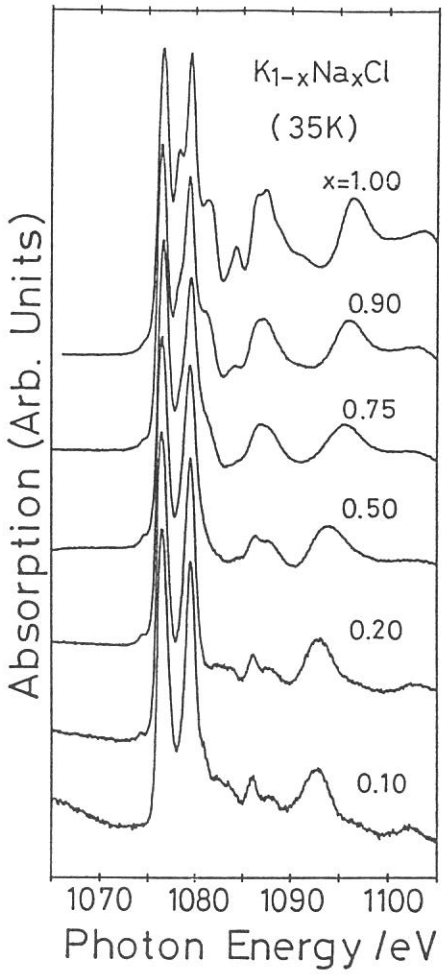

Fig. 2 Na K-XANES spectra of $K_{1-x}Na_xCl$ at 35K.

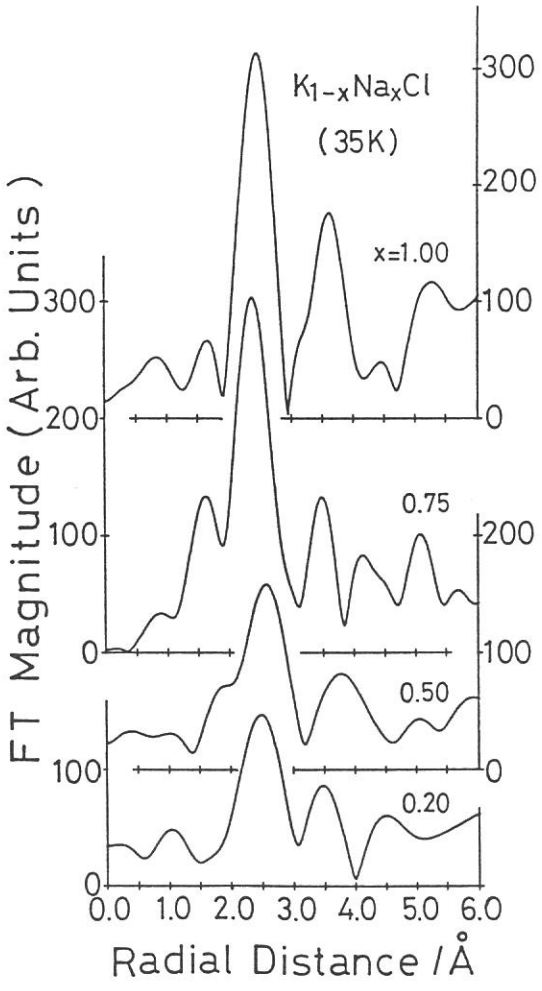

Fig. 3 Magnitude of Fourier transform of k^3 weighted Na K-EXAFS of $K_{1-x}Na_xCl$ at 35K.

References
1) T. Murata, T. Matsukawa, M. Mori, M. Obashi, S. Nao-e, H. Terauchi, Y. Nishihata, O. Matsudo, and J. Yamazaki, J. Phys. (France) 47, C8-107 (1986).
2) B. F. Sonntag, Phys. Rev. B11, 3601 (1974), S. T. Pantelides, Phys. Rev. B11, 2391 (1974).
3) T. Fujikawa, Private Communication.

EXAFS Study on Dehydration Process in $Mg(OH)_2$

Kazuya KAMON, Yasuo NISHIHATA, Hironobu NAONO,
Hikaru TERAUCHI and Takatoshi MURATA*

Faculty of Science, Kwansei-Gakuin University, Nishinomiya 662.
*Department of Physics, Kyoto University of Education,
Kyoto 612.

Magnesium hydroxide $Mg(OH)_2$ is dehydrated to magnesium oxide MgO at high temperature. The system of $(Mg(OH)_2)_{1-x}(MgO)_x$ has been studied by x-ray diffraction technique[1]. The characteristic reflections of $Mg(OH)_2$ disappear above the critical concentration $x_c(=0.68)$. Here we report the local structure around Mg atoms to clarify the microscopic mechanisms of the dehydration of $Mg(OH)_2$.

Fine powder samples of $Mg(OH)_2$ were dehydrated in vacuum. The degree of dehydration was determined from the weight loss of $Mg(OH)_2$ by means of vacuum electro-balance. The samples of $Mg(OH)_{2-2x}O_x$ with x=0.000, 0.220, 0.490, 0.681, 0.733, 0.896 and 1.000 were prepared by controlling temperature. The samples put on the first dinode of photo-multiplier. X-ray photo-electron yield spectra were taken near the Mg K edge by use of the EXAFS facility installed at the UVSOR BL-7A (beryl double crystal monochromator). Synchrotron energy was 750 MeV. The obtained spectra are shown in Fig.1. These spectra were analyzed by the same method as described in ref. 3. For the precise analysis, the nonlinear least square parameter-fitting method was applied.

The dehydration dependence of interatomic distance is shown in Fig.2. No significant point is seen in the figure. Since the structure of $Mg(OH)_2$ is CdI_2 type, and that of MgO is NaCl type, the coordination number of the first neighbor shells in $Mg(OH)_2$ and MgO are 6, while that of the second neighbor shell in $Mg(OH)_2$ is 6, and that of the second neighbor shell in MgO is 12. The ratio of coordination number N_2/N_1 is shown in Fig.3. The coordination number of first neighbor shell is decreased, while that of second neighbor shell is constant. The ratio N_2/N_1 increases from 1 to 2, as seen in the region $0<x<0.68$. When we consider the destruction of the $Mg(OH)_2$ layer structure in dehydration process in the region $0.68<x<1$. The coordination numbers of first and second neighbor shells increase, and the ratio N_2/N_1 is nearly constant. This result is consistent with the previous x-ray diffraction experiment.

We are indebted to all staffs of the UVSOR facility, especially to M.Watanabe, O.Matsudo, K.Fukui, J.Yamazaki and E.Nakamura for their continuous support and encouragement through the work.

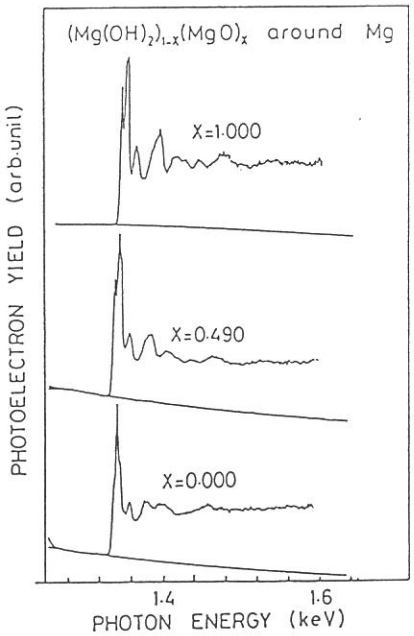

Fig.1 X-ray photo-electron yield spectra with x=1, 0.49 and 0.

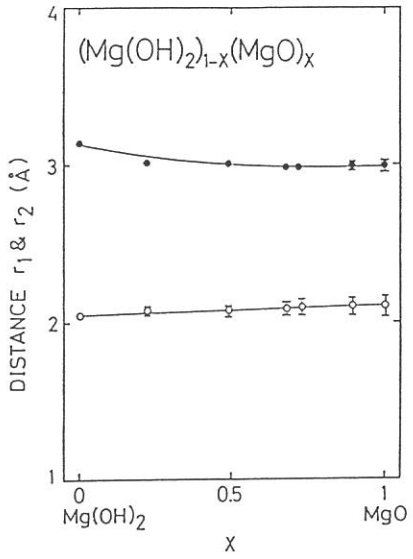

Fig.2 Dehydration dependence of interatomic distance.

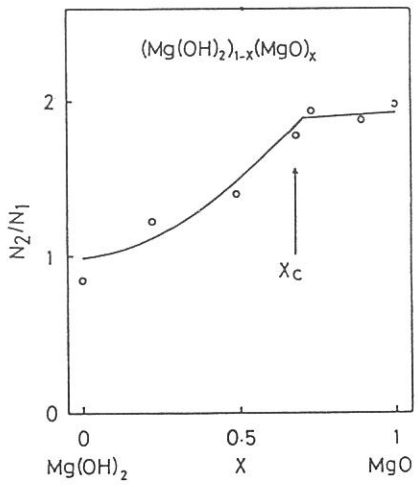

Fig.3 Dehydration dependence of coordination number ratio N_2/N_1.

References
1) H.Terauchi, T.Ohga and H.Naono:Solid State Commun. 35 (1980) 895.
2) Y.Nishihata, K.Kamon, H.Sakashita, H.Naono, H.Terauchi, T.Murata, S.Nao-e T.Matsukawa, M.Mori, A.Matsui and K.Mizuno:UVSOR Activity Report (1986) 46.
3) H.Maeda, H.Terauchi, K.Tanabe, N.Kamijo, M.Hida and H.Kawamura:Jpn. J. Appl. Phys. 21 (1982) 1342.

AUGER-FREE LUMINESCENCE FROM CsF, CsCl, CsBr, AND RbF AT RT

Shinzou KUBOTA,[1] Minoru ITOH,[2] Satoshi HASHIMOTO[3],
Jian-zhi RUAN(GEN),[1] and Shiro SAKURAGI[4]

(1) Rikkyo University, Nishi-Ikebukuro 3, Tokyo 171
(2) Department of Applied Science, Faculty of Engineering, Shinshu University, Nagano 380
(3) Kyoto University of Education, Fushimi-ku, Kyoto 612
(4) Union Material Inc., Tone-machi, Kitasoma, Ibaraki 270-12

We report the first direct evidence of the luminescence due to interatomic radiative transition of valence band electrons to outermost-core-hole states in alkali halides in which the band gap energy E_g is larger than the energy difference E_{vc} between the tops of the valence band and the outermost-core-hole state($E_g > E_{vc}$). This condition is fulfilled in CsF, CsCl, CsBr, RbF, and KF. We propose the term "Auger-free luminescence", emphasizing that this transition emits photons without ejecting Auger electrons.

Visible luminescence in CsF (2.5 - 5.6 eV), CsCl (3.9 - 6.0 eV), CsBr (4.4 - 6.2 eV), and RbF (2.6 - 6.2 eV) are observed at RT under 21.4 eV photon-excitation, corresponding to the interband transition from the outermost-core band to the conduction band. Fig.1 shows the luminescence yield excitation spectra for the 3.2 eV band(CsF), 4.5 eV band(CsCl), 4.9 eV band(CsBr) and 5.3 eV band(RbF). The most outstanding feature of the excitation spectra is that the threshold energies do not depend on halogen elements, but on alkali elements; the threshold energy E_{th} of CsF, CsCl, and CsBr is 14.1 ± 0.2 eV, and that of RbF is 17.0 ± 0.1 eV. These values are in good agreement with the outermost-core ionization energies of respective positive ions.

The observed threshold energies strongly suggest that the mechanism for the luminescence interested here is due to an interatomic Auger free transitions of electrons from X^- np halogen valence bands (n = 2, 3, and 4 for X = F, Cl, and Br, respectively) to the Cs^+5p or Rb^+4p holes.

By using band parameters determined by photoelectron spectroscopy,[1-3] the energy ranges of emitted photons due to Auger-free luminescence are calculated to be 2.6 - 4.3, 4.0 - 5.8, 4.4 - 6.2, and 4.3 -7.4 eV for CsF, CsCl, CsBr, and RbF, respectively. The agreement between measured and calculated values is good for three Cs-halides. We thus believe that the radiative transition occurs through the same band structure as determined by photoelectron spectroscopy. In RbF, the Auger-free luminescence is located approximately 1.7 eV lower than the calculated one. In order to explain this low-energy shift, it will be necessary to introduce some relaxation of the outermost-core-hole state, and/or the valence band state.

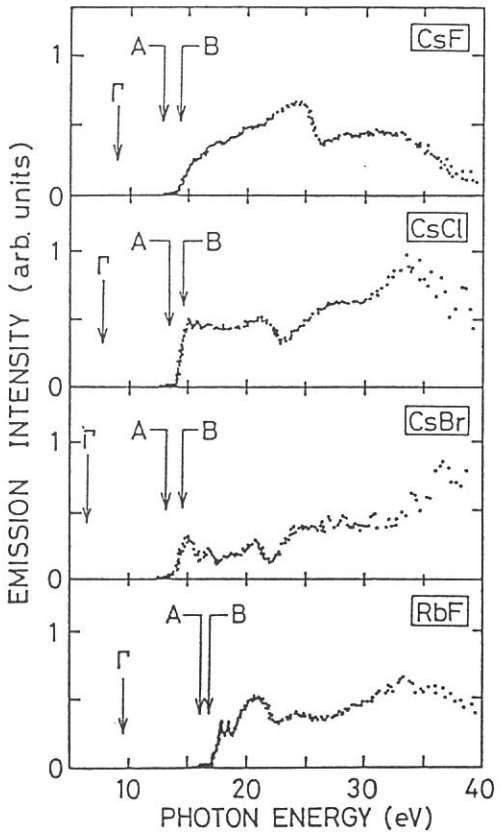

Fig. 1. Excitation spectra for the 3.2 eV band (CsF), 4.5 eV band (CsCl), 4.9 eV band (CsBr), and 5.3 eV band (RbF). Γ indicates the peak positions of the valence excitons, and A and B correspond to the core excitons of j = 3/2 and j = 1/2, respectively.

The intersting part of this work is that the low-energy shift is observed only in RbF and not in three Cs-halides. Further studies of this problem is needed.

It would be of interest to extend the present work in directions leading to the finding of other materials showing Auger-free luminescence, for example, KF, $BaBr_2$, $BaCl_2$, and BaF_2 as well.[3]

References

1. R.T.Poole, J.G.Jenkin, J.Liesegand and R.C.G.Leckey, Phys. Rev. B 11, 5179 (1975).
2. J.A.Smith and W.Pong, Phys. Rev. B 12, 5931 (1975).
3. M.Itoh, S.Hashimoto, S.Sakuragi and S.Kubota, Solid State Comm. in press.

Luminescence in KCl Irradiated with Undulator Light of UVSOR

Hideyuki NAKAGAWA, Toshiki DEGUCHI, Hiroaki MATSUMOTO,
Takeshi MIYANAGA*, Masami FUJITA**, Kazutoshi FUKUI***
and Makoto WATANABE***

Department of Electronics, Fukui University, Fukui 910
* Department of Physics, Faculty of Education,
Wakayama University, Sakaedani, Wakayama 640
** Maritime Safety Academy, Wakaba, Kure 737
*** Institute for Molecular science, Myodaiji, Okazaki 444

The defect production by radiation in alkali halide crystals has been studied extensively for many years. There is no report, however, on the production of defects under the wavelength selective and high-density excitation of inner core levels. It would be expected with such excitation to find out new defect centers and new production mechanisms. Semi-monochromatic and high-density excitation is now possible to be realized by using XUV-light from an undulator installed in an electron storage ring.

In the present study, KCl single crystals were irradiated with the undulator light which has the fundamental peak at 30 nm and the spectral width of about 5nm. On the irradiated crystals were performed measurements of absorption spectra from 180 nm to 900 nm and of emission spectra from 160 nm to 600 nm. Details of these experiments will be presented in another place.

In Fig. 1 is shown a typical example of the emission spectra measured at RT on the KCl crystals irradiated sufficiently with the above described undulator light. The emission spectrum consists of six or seven rather sharp bands located in the energy region from 4 to 6 eV. Each peak is situated with an equi-interval of 0.23 eV which is much larger than the typical phonon energies of KCl. These structures may be connected to the local vibration at the defect centers formated in the crystal. No discernible luminescence was observed at RT in the non-irradiated KCl crystals.

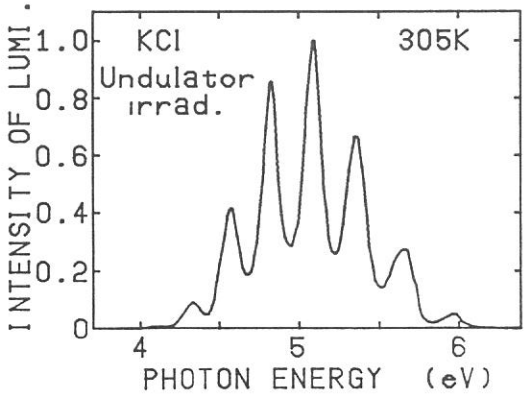

Fig. 1 Emission spectrum of KCl irradiated for several hours with undulator light.

Figure 2 shows the dependence of the intensity of luminescence on the irradiation dose of undulator light, which was obtained at RT

without changing all experimental set-up. The intensities of luminescence (L) are normalized with the values of electron beam current in the storage ring (I_B) which decrease gradually with time elapsing. The values of the irradiation dose represent those of the integrated area under the beam current vs. irradiation time curve. The normalized intensity of luminescence increases in proportion to the irradiation dose. Therefore, the luminescence shown in Fig.1 is reasonably associated to the defect centers created in the crystal by the undulator light irradiation.

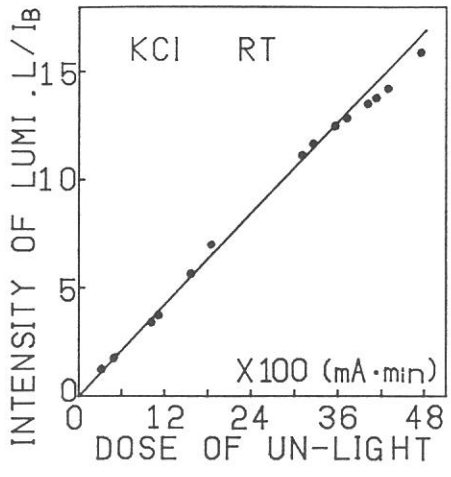

Fig. 2 Dependence of 5eV luminescence of KCl on the irradiation dose of undulator light.

The luminescence is observed rather strongly only in the temperature region between 280 and 350 K. The intensity decreases rapidly in both side above and below the region. This temperature dependence is difficult to understand, especially disappearance at low temperature, without considering some temperature dependent processes of energy transfer from the host lattice to the defect center.

Absorption spectra observed at RT in the crystals irradiated for 30 and 205 min are shown in Fig. 3. A band at 2.3 eV is due to F-centers and one arorund 6.2 eV is a new absorption band which is associated with the above described luminescence. The F-center production finishes in the early stage of irradiation, while the new defect centers go on growing with increasing the irradiation dose. The new center is supposed to be of the molecular type, though details are not revealed at present.

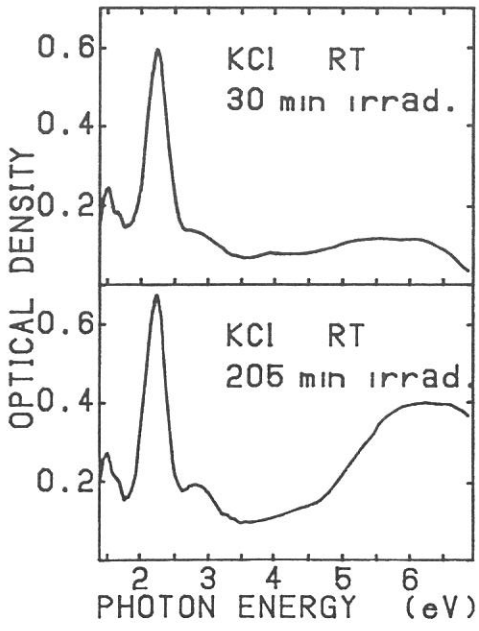

Fig. 3 Absorption spectra of KCl irradiated for 30 and 205 min with undulator light

Luminescence of Localized Excitons in KCl:Br

Ken-ichi KAN'NO, Koichiro TANAKA, Hideo KOSAKA, Osamu ARIMOTO*
and Yoshio NAKAI
Department of Physics, Kyoto University, Kyoto 606, Japan

Luminescence due to Br^- ions in KCl has been investigated at LHeT under excitation with UV light, by varying the amount of Br^- ions from 1.8×10^{-4} to 6.8×10^{-2} mole fraction. Excitation into the absorption band due to an isolated Br^- ion, which is known to locate at 7.46 eV,[1] does not induce any definite emission band. However, it was found that excitation into the low energy side of the Br^- band produces two distinct emission bands at 3.60 eV and 4.88 eV, as shown in Fig.1.

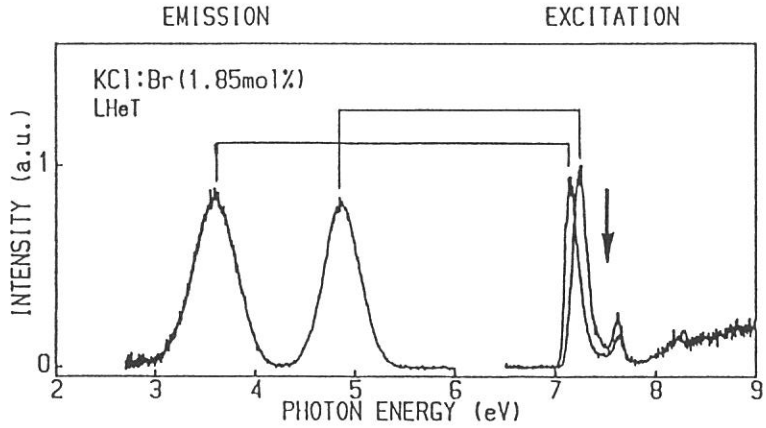

Fig.1. Emission (left side) and excitation (right side) spectra of KCl:Br at LHeT. The arrow shows the peak position of the localized exciton absorption due to an isolated Br^- ion.

These emission bands have been observed also by Wakita and Hirai under X-ray irradiation.[2] They assigned tentatively these bands to originate from localized excitons created at isolated Br^- ions. However, the fact that these emission bands are both stimulated strongly at the low energy tail of the impurity band suggests that they originate from impurity dimer centers.[3] Moreover, it has been confirmed that their intensities are both proportional to the square of Br^- contents over two orders up to 2×10^{-3} mole fraction.[4] This gives clear evidence that both emission bands derive from the dimers of bromine impurity.

---

* present address: Department of Physics, Okayama University, Okayama 700.

In order to clarify the nature of the initial states responsible for these emission bands, their decay characteristics have been measured under the single bunch operation of UVSOR by using the combination of a Seya-Namioka type monochromator at BL1B and a time-correlated single-photon counting system. An apparent time duration of the exciting light, measured by the present system, was 550 ps, and the interval of successive pulses was 177.6 ns. In Fig.2 is shown the decay behavior of the 4.88 eV emission, along with a pulse shape of exciting light at 7.25 eV. By a convolution analysis it was definitely determined that the emission decay obeys a single exponential function with the time constant 1.2 ns in more than 2 orders. This reveals that the 4.88 eV emission is the fluorescence from a singlet state. On the other hand, the 3.60 eV emission should be attributed to the phosphorescence from a triplet state because its life time is too long (of the order of μs) to be determined by the present measurements.

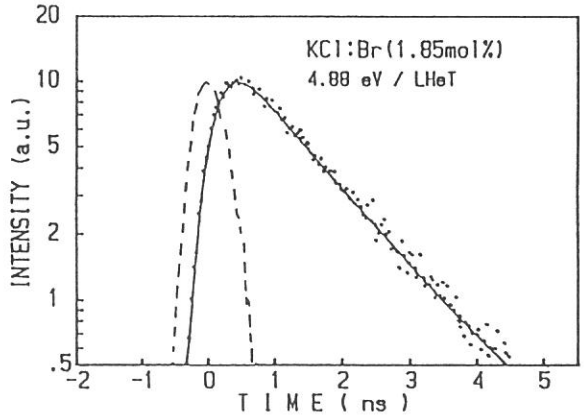

Fig.2. Decay curve of the 4.88 eV emission of KCl:Br at LHeT (dots), and pulse shape of the exciting light from UVSOR (broken curve). Fitting by the convolution analysis with time constant 1.2 ns is shown by solid curve.

On the analogy of π and σ emission from self-trapped excitons in pure alkali halides, it is supposed that the 3.60 eV emission originates from the lowest triplet state and the 4.88 eV emission from the higher singlet state of the $[Br_2^-(V_k) + e]$-relaxed excitons in the matrix of KCl. It is noteworthy that in KCl:Br excitons created at isolated Br^- ions decay non-radiatively even at LHeT, unlike the other halogen impurity systems.

1) D.Hinks and S.Susman: phys.stat.sol.(b)52 (1972), K53
2) S.Wakita and M.Hirai: J. Phys. Soc. Jpn. 24 (1968), 1177.
3) H.Nakagawa, M.Itoh and Y.Nakai: J. Phys. Soc. Jpn. 32 (1972), 1037.
4) K.Tanaka et al.: to be submitted.

TIME-RESOLVED FLUORESCENCE STUDIES ON LANGMUIR-BLODGETT FILMS OF BENZENE

Naoto TAMAI, Takaya YAMANAKA, Tomoko YAMAZAKI, Tadaoki MITANI, and Iwao YAMAZAKI

Institute for Molecular Science, Myodaiji, Okazaki 444

Photophysical and photochemical properties of benzene in ordered molecular assemblies such as Langmuir-Blodgett (LB) films are quite interesting in relation to the excited electronic and vibrational states. One can expect new aspects of photophysical processes in LB films different from those in gas phases, homogenious solutions, or crystals. LB multilayer films (Fig. 1) containing benzene chromophore, 15-phenylpentadecanoic acid (PPA), were deposited on CaF_2 or quartz plates at a surface pressure of 25 mN m^{-1}. Polystyrene films with different thickness were prepared for the comparison with LB films. Fluorescence spectra, lifetimes, and quantum yields were measured by the time-correlated, single-photon counting system equiped with Seya-Namioka monochromator in BL7B beam line of UVSOR.[1)]

As shown in Fig. 2, the LB film shows only a monomer-like fluorescence with a peak at 283 nm, while the polystyrene film shows an excimer fluorescence with a peak at 325 nm. Contribution of the monomer-like fluorescence increase in polystyrene film at 77K. Fluorescence spectral shapes were independent on the excitation wavelength from 170 nm to 250 nm. Fig. 3 shows a fluorescence decay curve of LB film excited at 190 nm, which is approximately single-exponential with a lifetime of 22 ns. This value is close to that of PPA in n-hexane solution. Above results indicate that, in LB film, ground-state geometry of benzene molecule is not a sandwich-type structure but may be L-shape or T-shape geometry, and further dynamical motion in the excited state is relatively restricted to form excimer. Fig. 4 shows excitation-energy dependence of fluorescence quantum yield (Φ_F). As the excitation energy is increased, Φ_F value is decreased sharply at 235 nm in polystyrene and 200 nm in LB film and has a minimum value at 190 nm (6.5 eV). The Φ_F value is recovered in higher energy region, indicating that the S_1 state

or the excimer state is produced directly through a benzene CT state in high energy excitation.[2)]

References

1) T. Yamanaka, M. Suzui, T. Horigome, T. Mitani, and I. Yamazaki, Ann. Rev. IMS, 138 (1985)

2) F. P. Schwarz and M. Mautoner, Chem. Phys. Lett., 85, 239 (1982)

Fig. 1 Schematic illustration of LB film

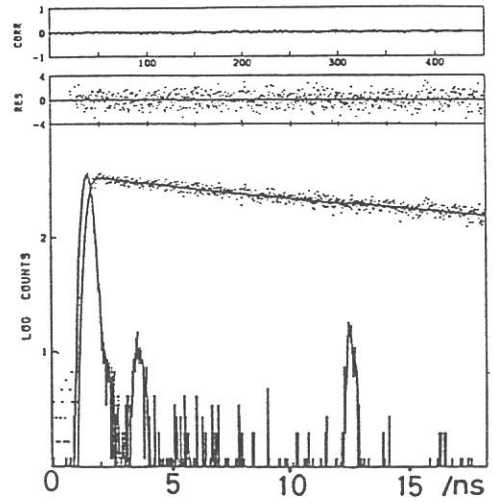

Fig. 3 Fluorescence decay curve of LB film excited at 190 nm and monitored at 280 nm

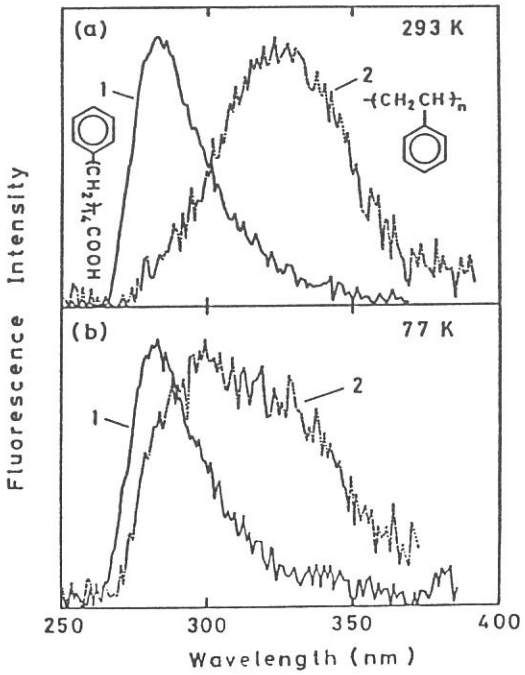

Fig. 2 Fluorescence spectra of LB film (1) and polystyrene (2) excited at 190 nm

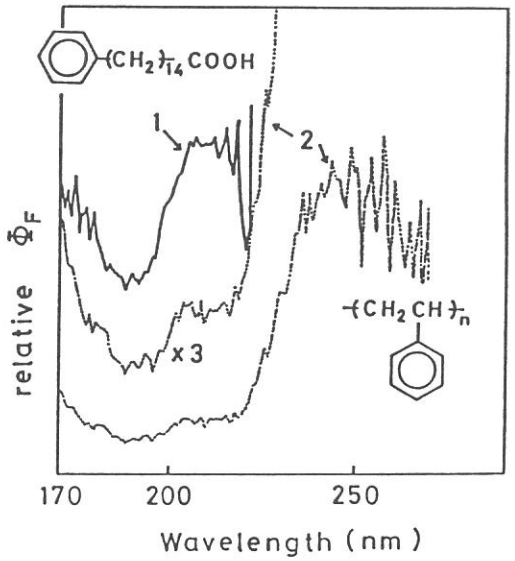

Fig. 4 Fluorescence quantum yields of LB film (1) and polystyrene (2) against excitation wavelength

Investigation of Energy Transfer in Tetracene-doped Anthracene Crystal by Photon-photon Coincidence Method

Tatsuhisa KATO, Takamasa MOMOSE and Tadamasa SHIDA

Department of Chemistry, Kyoto University, Kyoto 606

Energy transfer processes in organic molecular crystals have been investigated by coincidence method between the different wave length photons of luminescence signals at the temperature of 32K. The tetracene-doped anthracene microcrystalline layers were prepared by allowing a drop of benzene solution of anthracene and tetracene to evaporate on clean quartz disc.

The luminescence spectrum shown in Fig.1 was obtained under the illumination of the unfiltered SR light. The luminescence bands at 470nm and 680nm were assigned to fluorescence and phosphorescence of anthracene, respectively. The signal of tail of the spectrum around 550nm was due to the fluorescence of tetracene. Fig.2 shows the coincidence spectrum between the photon signals at the wave length of $\fallingdotseq$470nm and the greater wave length than 480nm, two coincidence peaks were shown definitely. In contrast to Fig.2, little time correlation between $\lambda \fallingdotseq$ 470nm photon and $\lambda > 620$nm photon was obtained as shown in Fig.3.

It is evident that two coincidence peak in Fig.2 correspond to the rise and decay fluorescence of anthracene and tetracene, respectively. It has been shown by Rojansky et al. [1] that the fluorescence lifetime of anthracene in tetracene-doped crystals decreased by orders of magnitude with increasing tetracene concentration, and the result was explained by the combined theory of exciton diffusion and long-range resonance energy transfer. The decay time of the first peak in Fig.2 is estimated about 900ps by the convolution of exponential function, and in agreement with their result of anthracene fluorescence decay. The slow rise and decay component of second coincidence peak in Fig.2 seems to correspond to the tetracene fluorescence, but the rise and decay time estimated of this component is much longer than expected by the direct energy transfer from anthracene to tetracene.

1) D.Huppert and D.Rojansky, Chem. Phys. Lett., 114(2), 149(1985).

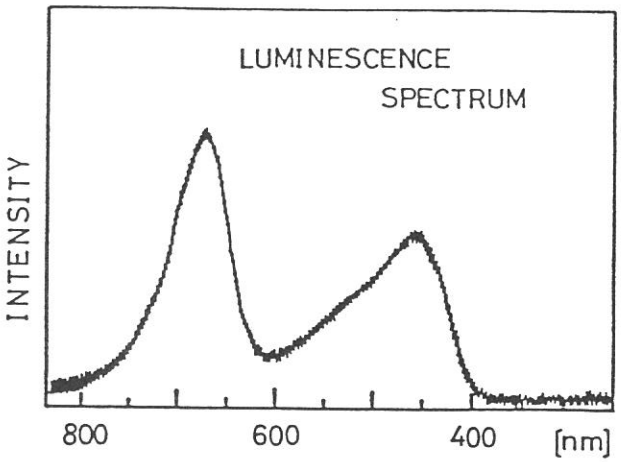

Fig.1
Luminescence spectrum of tetracene-doped anthracene crystal at 32k.

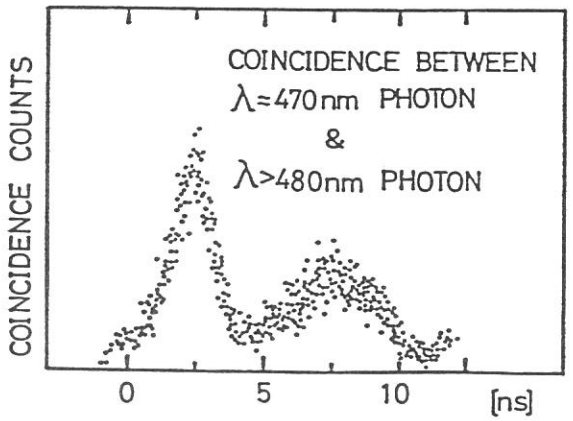

Fig.2
Coincidence spectrum between
$\lambda \fallingdotseq 470$nm photon and
$\lambda > 480$nm photon.

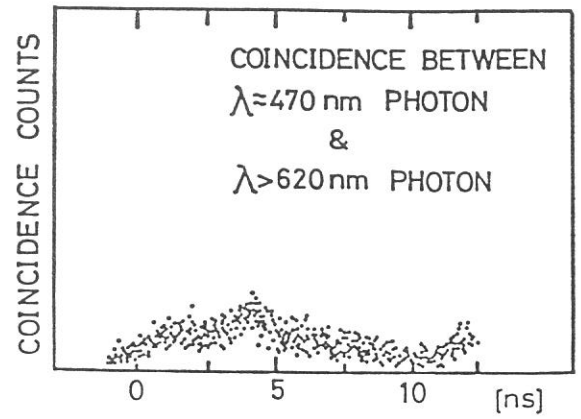

Fig.3
Coincidence spectrum between
$\lambda \fallingdotseq 470$nm photon and
$\lambda > 620$nm photon.

PHOTOCONDUCTIVITY THRESHOLD FOR ANTHRACENE IN SUPERCRITICAL XENON FLUIDS MEASURED AS A FUNCTION OF FLUID DENSITY

Kazumichi Nakagawa, Arisato Ejiri, Kengo Itoh
and Masaru Nishikawa

Department of Pure and Applied Sciences, University of Tokyo,
3-8-1 Komaba, Meguro-ku, Tokyo 153, Japan

Photoconductivity spectra of anthracene molecules were measured in supercritical xenon fluids as a function of fluid density. The purpose of the study is to gather informations on the solute-solvent interaction involved in photoionization processes. VUV light beam from a 1m Seya-Namioka monochromator was used with a wavelength resolution of about 0.8 nm. Photocurrent was measured by a Keithley 602 electrometer and was analyzed by a computer.

It has been shown that the photoconductivity spectrum near the threshold I_F can be fitted to the empirical formula[1], $(i/I)=B(E-I_F)^{5/2}$, where E is the photon energy, I the intensity of incident light, i the measured photocurrent. Fig. 1 shows a plot of $(i/I)^{2/5}$ vs E. Straight portion of the $(i/I)^{2/5}$ curve was extrapolated and the value of I_F was determined from its intercept on the base line. Fig. 2 shows a comparison of I_F obtained in this work with the result of calculation (curve A) according to the eq. 1;

$$I_F = I_g + V_0 + P, \qquad P = -e^2/2R(1-1/\varepsilon), \qquad (1)$$

where I_g is the gas phase ionization potential of anthracene, V_0 the conduction band energy in xenon fluids, P the polarization energy. P values were estimated by Born's formula with the dielectric constant ε calculated by the Clausius-Mossotti relation and with the radius R of anthracene$^+$ ion (0.325 nm) determined by Holroyd et al[1] from the Photoconductivity measurement in nonpolar hydrocarbon liquids. V_0 values are taken from experimental results by Reininger et

al.[2] I_g was reported to be 7.47 eV from the photoemission experiment.[3]

There is a clear difference between the calculated values of I_F (curve A) and observed I_F, especially at low densities. Validity of Born's formula was examined with the plot of ionic radii R estimated by eq. 1 utilizing V_0 data obtained by Reininger et al (Fig. 2(b)). Values of R at low densities decrease drastically with decrease in density, which may imply that there is stronger polarization than that estimated by Born's formula using the bulk dielectric constant. It is to be noted that R values at higher densities seem to converge at 0.325 nm, i.e. the value in nonpolar liquids. It seems to indicate that the local dielectric constant is higher than that of the bulk, hence the presence of clusters.

References: [1]R.A.Holroyd,J.M.Preses and N.Zevos, J.Chem.Phys. 79,483(1983).[2]R.Reininger,A.Asaf,I.T.Steinberger and S.Basak, Phys.Rev.B28,4426(1983). [3]R.Bosci,J.W.Murrell and W.Schmidt, Faraday Disc.Chem.Soc.54,116(1972).

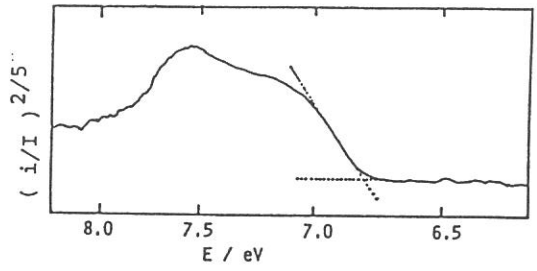

Fig.1. Plot of $(i/I)^{2/5}$ vs E.
Concentration of anthracene; ca. 10^{-3} M. Xe density; 2.42×10^{21} cm^{-3}.

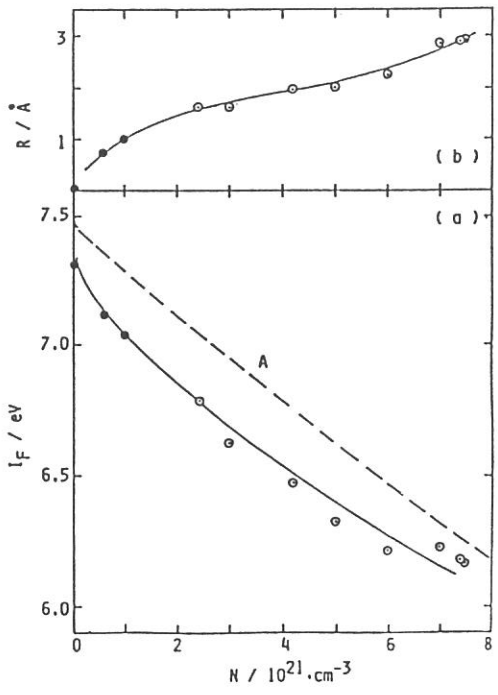

Fig.2(a). I_F vs Xe density N.
o :25°C, ● :110°C. Curve A;calculated (see text). (b).Radius R of anthracene$^+$ vs density N.

Angle-resolved Photoemission from Oriented Thin Films of Stearone with Synchrotron Radiation

N. Ueno, K. Seki*, N. Sato**, H. Fujimoto***, K. Sugita

and

H. Inokuchi***

Department of Image Science and Technology,
Faculty of Engineering, Chiba University, Yayoi-cho, Chiba 260

*Department of Materials Science, Faculty of Science,
Hiroshima University, Hiroshima 730

**Department of Chemistry, College of Arts and Sciences,
The University of Tokyo, Komaba, Meguro, Tokyo 153

***Institute for Molecular Science, Myodaiji, Okazaki 444

The angle-resolved photoemission spectroscopy (ARUPS)is an unique tool in investigating the energy band dispersion of solids in wide energy range. Further, using this technique, we can obtain the information of molecular orientation in very thin film of molecular solids with little radiation damage.

Our purpose of this study is (i) to clarify the existence of the energy band dispersion E=E(k) in a long chain molecule and (ii) to study the molecular length which is necessary for the appearance of the dispersion. In this direction, we determined E=E(k) relation in a repeating $-(CH_2)-$ chain[1] using hexatriacontane thin films and LB-films of cadmium arachidate.

Here, we report the results of the angle-resolved photoemission experiment on thin films of stearone, $CH_3(CH_2)_{16}CO(CH_2)_{16}CH_3$, using synchrotron radiation as a tunable light source. This molecule has shorter 'effective chain length', that is $(CH_2)_{16}$, than those used in the previous work[1].

The thin films of about 9nm thickness were prepared on Mo substrates by vacuum evaporation in the preparation chamber and subsequently transferred to the measurement chamber. The molecular orientation of the thin films was studied by measuring ARUPS spectrum as a function of emission angle of photoelectrons, and we found that the molecules stand as their long axes perpendicular to the substrate surface.

Figure 1 displays an example of the photon energy dependence of the normal emission spectrum in the photon energy range 40 - 120 eV. Using these results, E vs k curves were calculated in

accordance with the previous work,[1] and shown in Fig. 2. Here the curves are plotted in the extended zone scheme, since an unclarified energy shift exists depending on the photon energy for $h\nu \lesssim 70$eV and $h\nu \gtrsim 105$eV. A modified result of an ab-initio band calculation for an idealized polyethylene chain is compared[1] in the range $3.72\text{cm}^{-1} \lesssim k \lesssim 4.96\text{cm}^{-1}$, where the $h\nu$-dependence of the unclarified energy shift is small. Excellent agreement was obtained between observed and theoretical dispersion relations. We note that all valence band dispersion was clearly observed for $(CH_2)_{16}$ chain and especially the upper B_1 band near the top of valence bands, which was not observed in the previous work[1], was clearly found.

References

1) K. Seki, N. Ueno, U. O. Karlsson, R. Engelhardt, and E. E. Koch, Chem. Phys. 105, 247 (1986), and references therein. H. Fujimoto, T. Mori, H. Inokuchi, N. Ueno, K. Sugita and K. Seki, Chem. Phys. Lett., 141, 485 (1987).

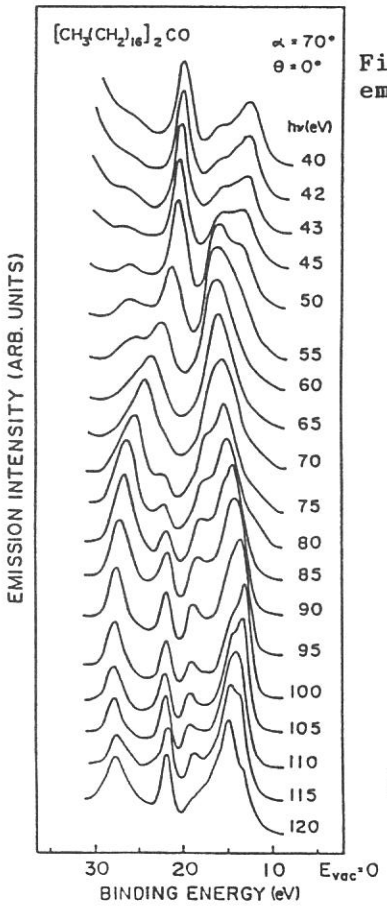

Fig.1 Photon energy dependence of normal-emission photoelectron spectra of stearone.

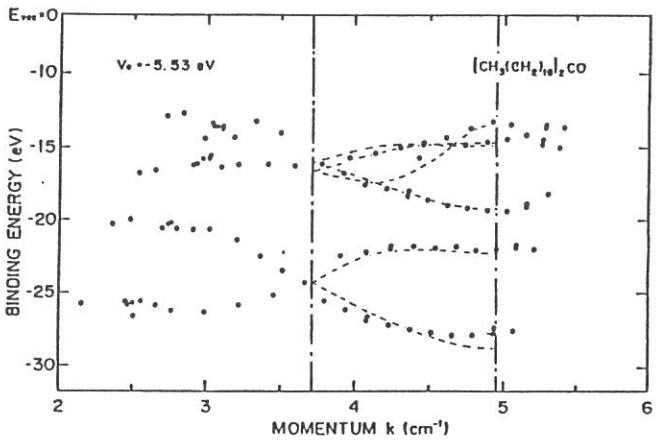

Fig.2 Energy-band dispersion of stearone.

ULTRAVIOLET PHOTOEMISSION STUDY OF POLYTHIOPHENE OLIGOMERS (I)

H. Fujimoto, K. Seki,* U. Nagashima, H. Nakahara,**
J. Nakayama,** M. Hoshino,** K. Fukuda,** and H. Inokuchi

Institute for Molecular Science, Myodaiji, Okazaki 444
**Department of Materials Science, Faculty of Science, Hiroshima University, Hiroshima 730*
***Department of Chemistry, Faculty of Science, Saitama University, Urawa 338*

Conducting polymers are the subject of recent active researches. However, structural characterization is quite limited by their amorphous nature and by their insolubility to solvents. By use of oligomers these problems are overcome, although the end effect arises. Polythiophene belongs to the class of conducting polymers with non-degenerate ground state and its electronic structure is of great interest.

We will report here on the ultraviolet photoelectron spectroscopic (UPS) study of several polythiophene oligomers; 2,2':5',2":5",2"':5"',2"":5"",2""':5""',2""":5"""-septithiophene (α_7), 2,2':5',2":5",3"':4"',2"":5"",2""':5""',2""":5"""-septithiophene ($\alpha_3\beta\alpha_3$), and (E)-1,2-bis(2,2':5',2"-terthiophene-5-yl)ethylene ($\alpha_3V\alpha_3$).

Thin films of 30-50 nm thickness were prepared by *in situ* vacuum evaporation in the preparation chamber and subsequently transferred to the main chamber.[1] UPS spectra were measured for the normal emission from the sample surface with the incident angle of the light beam of 60°.

Figure 1 shows the photon energy ($h\nu$)-dependent UPS spectra of α_7. In the low-binding-energy region (E_b = 2 - 4 eV) the π-bands are observed, while the peak located at around E_b = 7.5 eV has a σ-character. The ionization cross section of the p electron is almost constant in this region and that of the s electron decreases gradually with increasing $h\nu$. As the result, the relative intensity of π bands increases with $h\nu$.

Figure 2 shows UPS spectra of $\alpha_3\beta\alpha_3$ and $\alpha_3V\alpha_3$ and the orbital energy calculated by the semiempirical MNDO method. The agreement between UPS spectra and the calculated energy is good. It should be mentioned that from the optimized geometry by MNDO $\alpha_3\beta\alpha_3$ consists of the two planar α_3 parts and the β ring, which the α_3 and β parts are perpendicular to each other. Correspondingly, the π-band spectrum of $\alpha_3\beta\alpha_3$ can be reproduced by adding the spectra of two trimers and a monomer.

These results clearly indicates that the way of polymerization significantly affects the electronic and electric properties of polythiophene, and the controll of the polymerization process is important for achieving good conductivity.

Further investigation is in progress on other oligomers containing 3-8 thiophene rings.

Reference

1) K. Seki, H. Fujimoto, T. Mori, and H. Inokuchi, UVSOR Activity Report, **14**, 11 (1986).

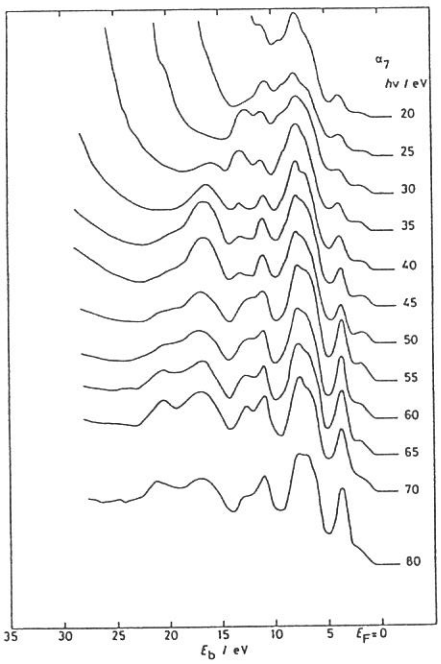

Fig. 1 $h\nu$-dependent UPS Spectra of α_7.

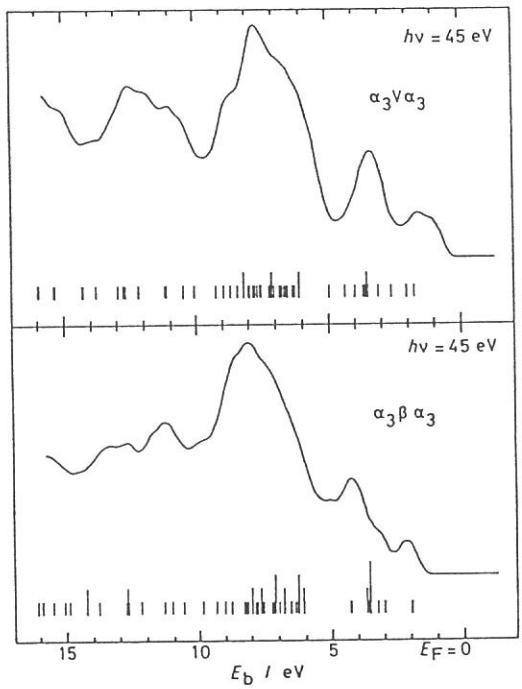

Fig. 2 UPS spectra of $\alpha_3\beta\alpha_3$ and $\alpha_3V\alpha_3$. Vertical lines show the orbital energy calculated by MNDO.

SYNCHROTRON RADIATION EXCITED CHEMICAL VAPOR DEPOSITION OF THE CARBON FILMS

Akira YOSHIDA*, Yoji SAITO*, Katsushi INOUE*,
Haruhiko OHASHI*, Hiroshi OGAWA, Kosuke SHOBATAKE*****

* Toyohashi University of Technology

** Saga University

*** Institute for Molecular Science

Photo-chemical vapor deposition (Photo CVD) is a promising method of new fabricating processes and selective growth at low temperature. Synchrotron radiation (SR) is a suitable light source for photo CVD process, because many reactant gases have large dissociation and ionization cross sections in the VUV region. In this study, hydrogenated carbon (C:H) films were deposited on Si substrates by SR-CVD using C_4H_{10} gas at room temperature. The mechanism of the deposition and the optical properties of the films are investigated.

Electric field ranged from -120 V/cm to +170 V/cm was applied during the deposition as illustrated in Fig.1, where a Ni mesh was fixed at 0.7 cm upstream from the substrate. A direction of the positive electric field was defined from mesh to substrate. The gas pressure was kept below 1 Torr. The accumulated light intensity was upto 500 mA hr.

Optical emission from excited C_4H_{10} gas was observed in the visible region (Fig.2). It is found that CH, C_2 radicals and H atoms exist.

Fig.3 shows SEM image of the sample. The film was selectively grown on the SR irradiated region. The dependence of thickness on the applied electric field is shown in Fig. 4. When a positive bias is applied, thickness of the film is proportional to the applied voltages. However the thickness of the films keep a fixed value independent of the negative electric field. Therefore, not only the positive ions but also the neutral species contribute to the deposition of the films. Infrared (IR) absorption spectra of the film was shown in Fig. 5. The observed peaks correspond to sp^3 CH_3 at 2960 cm^{-1}, sp^3 CH_2 at 2920 cm^{-1}, sp^3 CH_3 at 2880 cm^{-1}, sp^2 CH at 3000 cm^{-1}. It is evident that the films were sp^3 rich C:H films.

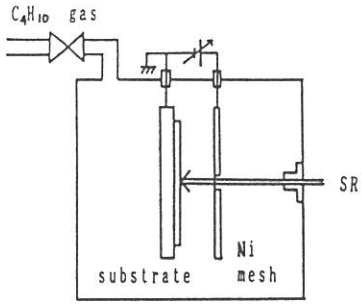

Fig.1 Reaction Chamber

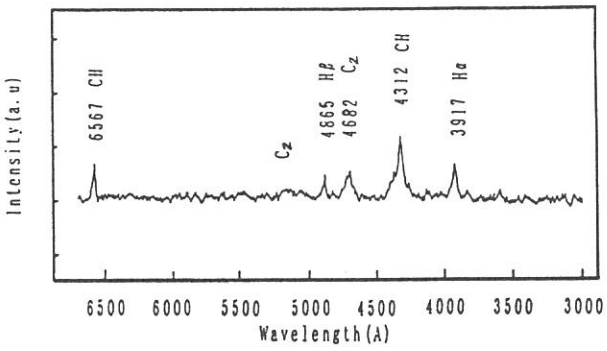

Fig.2 Optical emission spectrum in visible region of C_4H_{10}

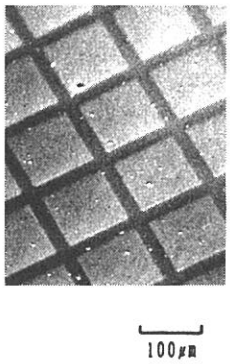

Fig.3 SEM image of the deposited film

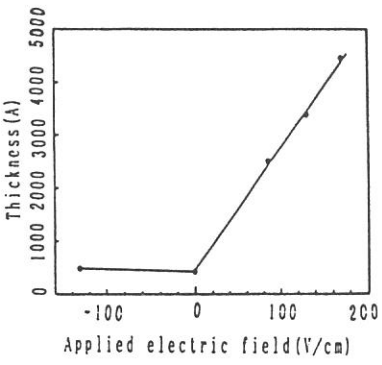

Fig.4 The dependence of the thickness on the applied Electric field

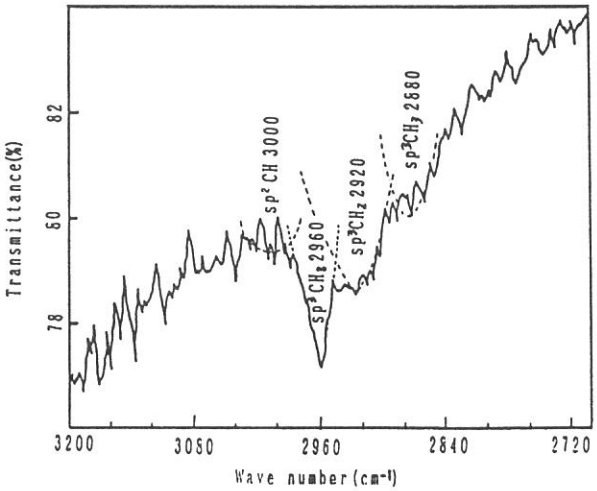

Fig.5 IR absorption of the film

WAVELENGTH DEPENDENCE OF SELF DEVELOPMENT OF POLYMETHYLMETHACRYLATE

HITOMI YAMADA, SATOSHI ITOH, MAKOTO NAKAMURA, HISATO KATOH, SHINZO MORITA and SHUZO HATTORI
Department of Electronics, Nagoya University
Fro-cho, Chikusa-ku, Nagoya 464 (Japan).

Polymethylmethacrylate (PMMA) was exposed to synchrotron radiation (SR) directly or through Be film as an X-ray filter. The typical wavelength was ranged in 3-1000Å for the direct exposure and in 3-20Å for the exposure through Be film. The SR exposure was performed at an electron energy of 750MeV. The substrate temperature could be controlled from RT to 300℃ by using a temperature controller. The molecular structure before and after exposure was investigated by IR and UV measurements.

Self development characteristics of PMMA are shown in Fig.1 as a function of exposure dose. It was found that the self development was remarkably affected by substrate temperature. Self developing thickness increased with increasing the exposure dose at a small dose, while it saturated at a large dose without substrate heating. However, the self development was reached to the bottom by substrate heating. Then, it was found that the self developing rate was dependent on substrate temperature. With increasing the substrate temperature, the self developing rate was enhanced. For the direct exposure, the self development to the bottom was obtained at the temperature over 100℃ near the glass transition temperature. On the other hand, it was attained below 100℃. Therefore, it is considered to be possible that the pattern fabrication can be easily obtained by SR exposure with the substrate heating.

The IR spectra before and after SR exposure are shown in Fig.2 for both exposure conditions at the substrate temperature of RT. The absorption peaks at 1730 and 1140cm^{-1} due to ester and carbonyl structure decreased with increasing the exposure dose for both conditions. For the direct exposure, the hydrocarbon film was finally formed as a residue. Then, the new peaks around 1700cm^{-1} due to the oxidized C=C structure was observed[1]. However, it was not clearly observed for the exposure through Be film. From the results of UV measurement, it was found for the direct exposure that the residual film resembled a graphite carbon film.

References

[1] M. Shen, "Plasma Chemistry of Polymer" (Marcel Dekker, New York., 1976).

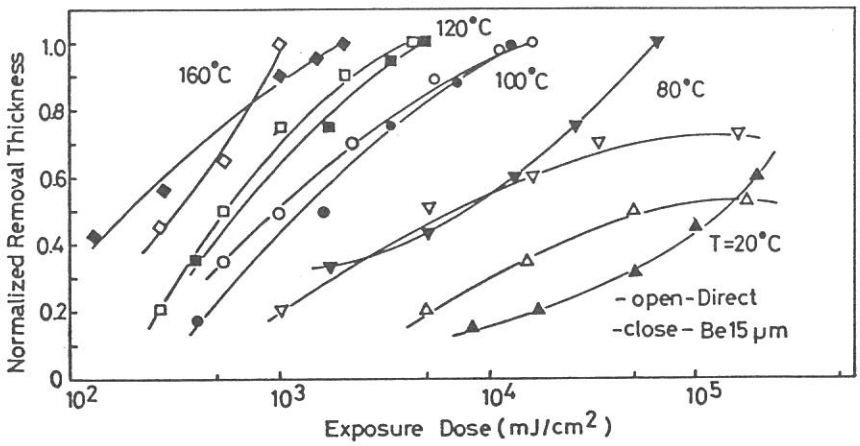

Fig.1. Dependence of self development on substrate temperature.

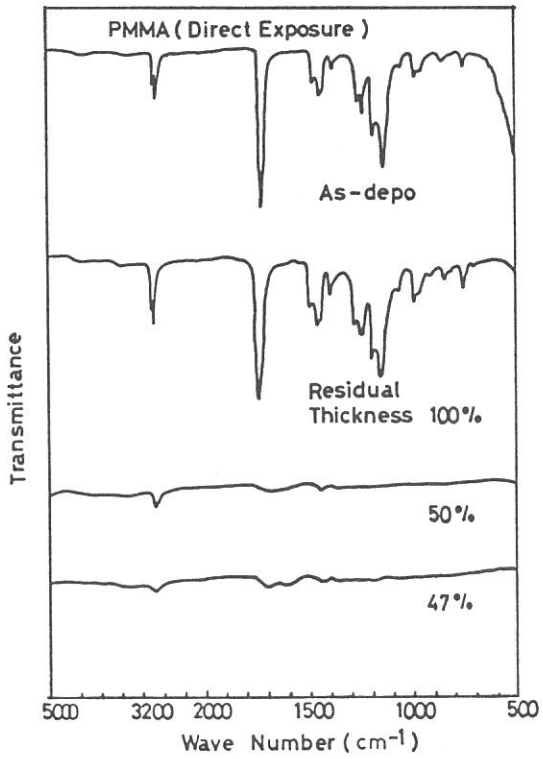

Fig.2(a). IR spectra before and after SR direct exposure.

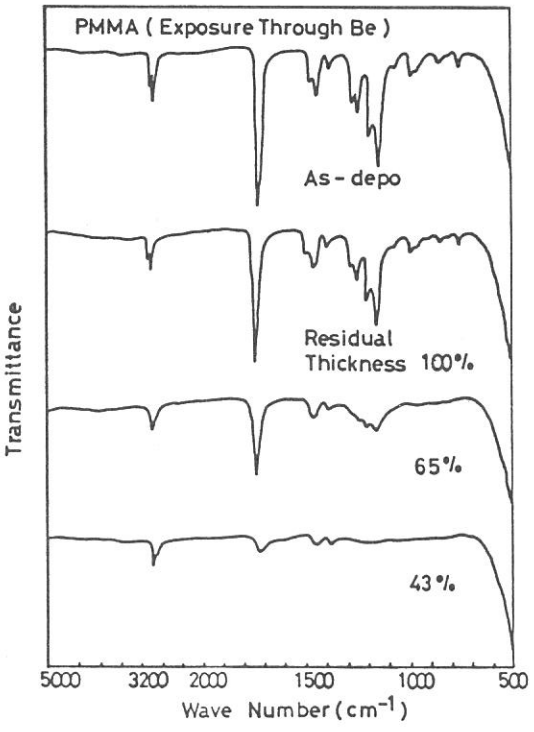

Fig.2(b). IR spectra before and after SR exposure through Be.

RADIATION-INDUCED DEGRADATION OF MOS DEVICES

Akira YOSHIDA, Hiroyuki SUETSUGU, Tetsuya HIRANO,
Yoji SAITO, Hisao KATO*
Toyohashi University of Technology, Toyohashi,440
* Nagoya Municipal Research Institute,Nagoya,456

Synchrotron radiation (SR) lithography has attracted much attention recently. Replication of high-resolution patterns is possible due to the high collimation of SR. In the next semiconductor technology,SR lithography will be widely used. Mask and resist materials for this process have been reported. But SR irradiation effect in the semiconductor devices have not been investigated. In this report, we show SR irradiation effect for $Au/SiO_2/Si$ MOS diodes, and its annealing effect.

The thickness of SiO_2 layer on n-type (100) Si wafer was 20nm. Metal electrode of Au was deposited on the SiO_2 layer. (Fig.1). Fig.2 represent the typical Capacitance-Voltage characteristics before and after irradiation. Hysteresis and flat-band voltage shift were observed in the C-V characteristics after SR irradiation. Interface states density (N_{ss}) of MOS diode increased by SR irradiation. Electron-hole pairs are formed in the SiO_2 layer by SR irradiation and the holes would be trapped near the interface between SiO_2 and Si,making up the space-charge.

The MOS diodes after SR irradiation were annealed at 50℃-250℃ during 60 minutes in the N_2 atmosphere. Fig.3 shows the relationship between annealing temperature (T_A) and flat-band voltage shift (ΔV_{FB}). The ΔV_{FB} almost disappeared at 250℃.

Fig.4 shows the relationships between N_{ss} and T_A. The hysteresis width also disappeared at 250°C. The N_{ss} almost went back to the original value of MOS diodes before SR irradiation at 250°C.

In summary, the damages are produced by SR irradiation in the semiconductor devices, but they are easily removed at 250°C.

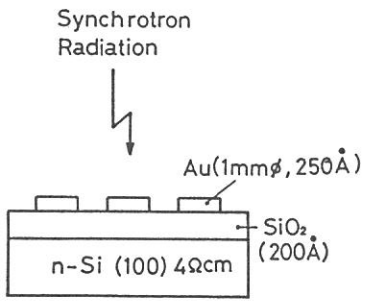

Fig.1 Sample(MOS diode)

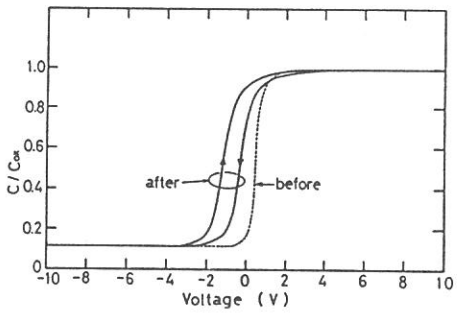

Fig.2
Capacitance-Voltage characteristics

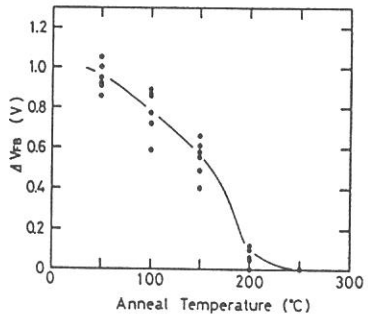

Fig.3
Dependence of flat-band voltage shift on annealing temperature

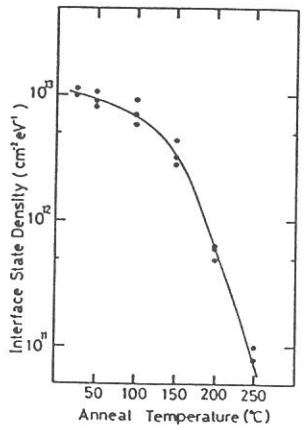

Fig.4
Dependence of interface states density on annealing temperature

Fabrication and its Focal Test of a Free-standing Zone Plate at VUV Region

Hiroshi Kihara[1], Yoshio Shimanuki[2], Kenzo Kawasaki[2], Yutaka Watanabe[3], Shigetaro Ogura[3], Hirotsugu Tsuruta[4], and Yoshinori Nagai[5].

1) Jichi Medical School, School of Nursing, Minamikawachi, Tochigi 329-04, Japan
2) Department of Oral Anatomy, School of Dental Medicine, Tsurumi University, Tsurumi 2-1-3, Yokohama 230, Japan
3) Canon Research Center, CANON INC., Morinosato-Wakamiya 5-1, Atsugi, Kanagawa 243-01, Japan
4) Department of Materials Science, Faculty of Science, Hiroshima University, Hiroshima 730, Japan
5) Laboratory of Molecular Biolgy, School of Veterinary Medicine Azabu University, Fuchinobe, Sagamihara, Kanagawa 229, Japan

Many efforts have been done for the development of X-ray microscopy in the wavelength between 2.37 and 4.47 (nm) (absorption edges of oxygen and carbon, respectively), because of high contrast of biological materials against water. In longer wavelength region, however, relatively less efforts heve been paid. We have studied feasibility to sort out the importance of the development of X-ray microscopy in longer wavelength region, and pointed out possible effectiveness of the utilization of VUV light, such as the use of phosphor absorption edge [1,2].

To develop the X-ray microscope at the wavelength of VUV region, the use of a free-standing zone plate is inevitable. Thus, we have fabricated a free-standing zone plate, and tested its focal and magnifying features at the Institute for Molecular Sciences (Okazaki). The test system was applied for the observation of mesh and hard tissues (bones and teeth).

Fabrication procedure of zone plate

Original fabrication procedure was reported elsewhere [1]. It was improved in several points. The present characteristics are: n=312, f=150 (mm) at 8 (nm) of the light, dr_n=0.98 (μm), and thickness of Au = 2 (μm) with a central mask of 0.2(mmϕ) was employed.

Test system of zone plate

Focal and magnifying features of the fabricated free-standing zone plate have been tested at the beam line 6A2 of UVSOR at the Institute for Molecular Sciences. The zone plate was placed at the downstream of a plane-grating monochromator through which monochromatized lights from 8 (nm) to visible region are utilized. Beam from the monochromator was focused with 1 (mm) square, and diverged with 10 (mmϕ rad). Photons passing through a pinhole were used for the experiments. Samples (meshes or hard tissues) were fixed directly on a pinhole with silver-paste. Magnifying ratio was changed by removing distances between the zone plate and detectors. To detect the focused images, multichannel plate (Hamamatsu Photonics, MCP-F2222) [3] or

photographic films (MEM, Mitsubishi) were used.

Results

In Fig. 1, a photograph of an image of Cu 25 (μm) mesh (TAAB Lab. Equip.) is shown. The mesh was mounted on 0.4 (mmφ) pinhole. MEM films were used to detect images focused by the zone plate. The observed wavelength was 10.5 nm. Magnifying power was set at 10. The dark parts on the upper left are due to 0-order diffraction, and a mesh image at the center is due to first-order diffraction. Judging from the sharpness of mesh edges, resolution of a few microns is attained, which is comparable to grain size of the film. The mesh images were defocused with the increase of the wavelength of the incident beam.

Hard tissues (bones and teeth) were observed. An example of a human thigh bone with many small holes (bone cavities) is shown in Fig. 2. The area other than cavities gave scarce information, probably because of its thickness (c.a. 40 μ). A technique to prepare thinner specimen is necessary.

References

1. Y. Nagai, Y. Nakajima, Y. Watanabe, S. Ogura, K. Uyeda, Y. Shimanuki,and H.Kihara:in "X-ray Microscopy.Instrumentations and Biological Applications (ed. by P.C. Cheng and G.J. Jan)", in press, Springer-Verlag (1987)
2. P.C. Cheng, H.B. Peng, K.H. Tan, J.Wm. McGowan, R. Feder, D.M.Shinozaki:in "X-ray Microscopy (ed. by G. Schmahl and D. Rudolph)", pp.285-293, Springer-Verlag (1984)
3. S. Matsuura, S. Umebayashi, C. Okuyama and K. Oba: IEEE Trans. Nucl. Sci., NS-32, 350-354 (1985)

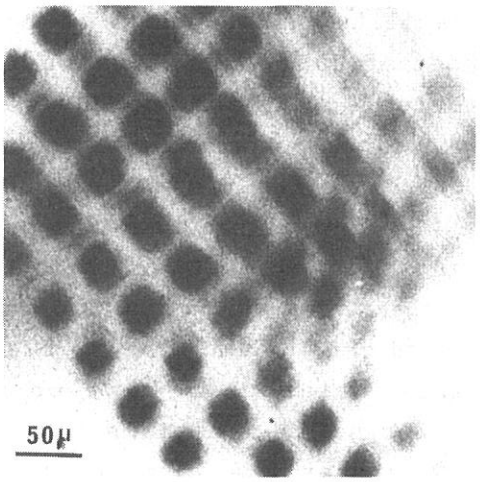

Fig. 1. Cu 25(μm) mesh pattern. The picture was taken with 10-fold magnification. 94.8 (nm). 2 hours with MEM film.

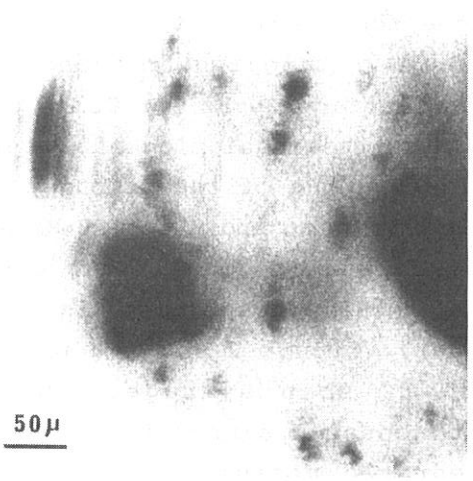

Fig. 2. Compact bone of human thigh with Haversian canals (big black holes) and bone cavities (small holes). The picture was taken with MEM film for 210 (min). 9.48 (nm).

Far-infrared Photoacoustic Spectroscopy; Detection System

T.Masujima[1], T.Nanba[2], K.Fukui[3], H.Yoshida[1] and M.Watanabe[3]

1. Institute of Pharmaceutical Sciences, Hiroshima University School of Medicine, Kasumi 1-2-3, Hiroshima 734
2. Department of Physics, Faculty of Science, Tohoku University, Sendai 980
3. Institute of Molecular Science, Myodaiji, Okazaki 444

The photoacoustic method is originated to the finding by A. G. Bell and detects the heat generation accompanied by the electromagnet wave absorption.[1)] In addition to the normal wave range such as UV, visible and near- and mid-IR regions, X-ray photoacoustic effect was recently observed using synchrotron radiation source.[2)] Photoacoustic method detects the pressure wave which was generated by heat expansion of the surrounding gas close to the surface of materials. Thus, this indirect detection principle enables us to apply this method to any range of wavelength with a same detector. Far-IR is the longer end of these region with a lot of interesting research fields.

Air-tight photoacoustic cell was made of stainless steel and set at the focus point of far-infrared facility(sample point) at beam line 6A1. Chopping frequency was set at 40Hz for photoacoustic detection and 20 Hz for Goley cell detection. Soft springs were used for the insulation of the surrounding acoustic noise. Figure 1(a) shows one of the strongly contributed noise from the turbomolecular pump and this 120 Hz noise was disappeared when the pump was stopped as seen in the usual noise level of Fig. 1(b). The spiked noise whose source is still unclear was cut off by low-pass filter. Figure 2 shows a photoacoustic signal of silver black with 32 scan average. The convex triangular rise-up of photoacoustic signal is the typical for solid materials to show integrated rising up of the temperature at the surface of the sample. The signal by Goley cell(Cathodeon Ltd. England)(Fig.3) shows quite different and smooth shape which may due to some

modification through electronics and showed better S/N ratio than that for photoacoustics at this stage. The improvement of the sensitivity of this detection system is under the the progress in our group.

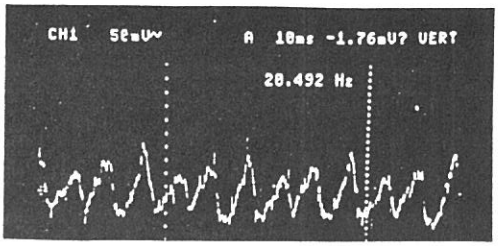

Figure 1a. A signal from microphonic photoacoustic cell without Far-IR beam when the turbo-molecular pump was running.

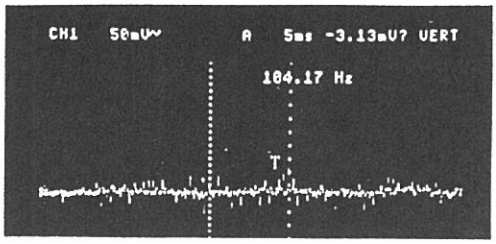

Figure 1b. A signal same to fig.1a without the pump operation.

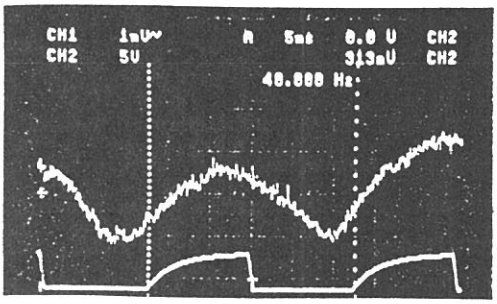

Figure 2. A photoacoustic signal of silver black at 40 Hz chopping. Upper signal; photoacoustic signal with 32 scan average, lower; chopping signal from light chopper.

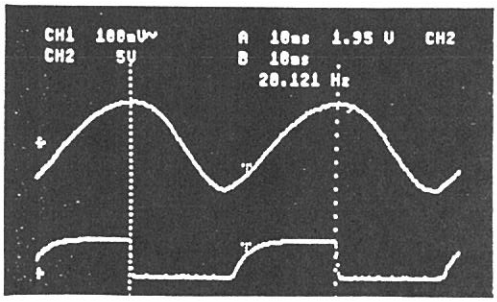

Figure 3. A signal for Goley cell detection at 20 Hz chopping (8 scan average).

References

1. A.G.Bell, Am. J. Sci., 20, 305 (1880).
2. T.Masujima, "Photoacoustic X-ray Absorption Spectroscopy" in "Topics in Current Chemistry" Vol. 147 ("Synchrotron Radiation in Chemistry and Biology II") ed. by E. Mandelkow, Springer-Verlag, Heiderberg in press.

Effect of temperature on the far-infrared optical constants of liquid acetonitrile

Tetsuhiko OHBA, Hironori SUZUKI and Shun-ichi IKAWA

Department of Chemistry, Faculty of Science,
Hokkaido University, Sapporo, 060

The far-infrared optical constants of liquid acetonitrile were measured in the temperature range 238K - 343K by use of a far-infrared spectrometer at BL6A1.

The liquid sample was sealed in a liquid cell with O-rings. An aluminium spacer of 30μm thickness and silicon windows of 25mm diameter and 3mm thickness were used. The cell was attached to a copper block whose temperature was controlled by use of an electric heater and a cooled nitrogen gas. The observed transmission spectra of liquid acetonitrile at temperatures 238K to 343K are shown in Fig.1. The periodic waves on the spectra are interference fringes due to the multiple internal reflection. For an analysis of these 'deformed' spectra, we have developed a computer simulation program based on the optical theory allowing for the multiple internal reflection and the Kramers-Kronig relation.[1] An example of the best fits obtained by the simulation is shown in Fig.2.

The temperature dependence of the absorption coefficients of liquid acetonitrile is shown in Fig.3. According to a fluctuating cage model,[2] the lump at around 30cm^{-1} is

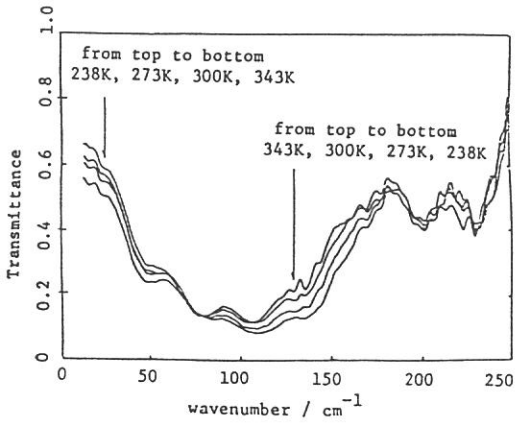

Fig.1. Observed transmission spectra of liquid acetonitrile.

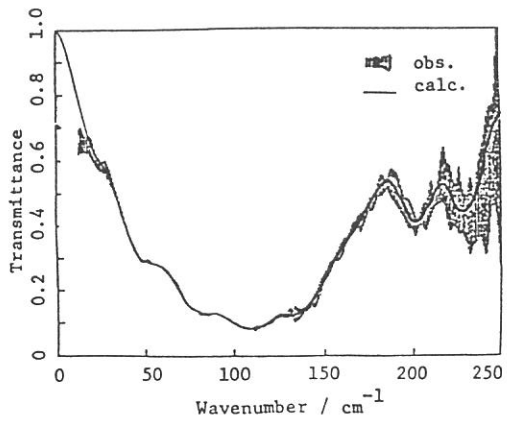

Fig.2. Observed and calculated transmittances at 238K.

caused by relaxation of the cage in which the liquid molecule performs the librational motion. The increase of the lump with temperature indicates the faster decay of the cage at the higher temperature. Fig.4 shows the rotational velocity correlation function given by the Fourier transform of the absorption spectrum. With increasing temperature, the oscilation amplitude of the correlation fuction decreases. This fact is also explained by loosening of the cage at the higher temperature.

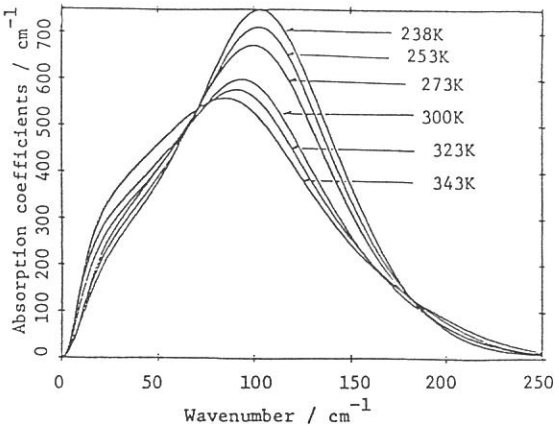

Fig.3. Absorption coefficients at temperatures 238K - 343K.

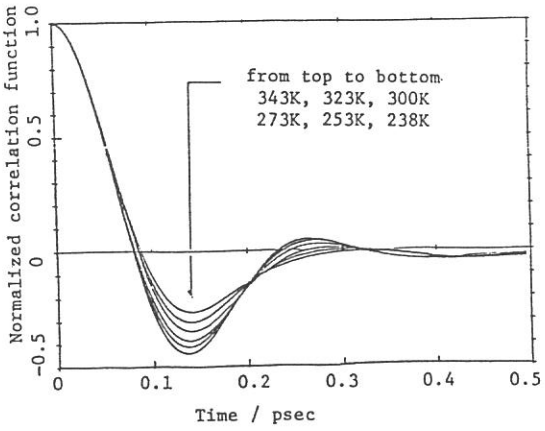

Fig.4. Rotational velocity correlation function.

References

1) T.Ohba and S.Ikawa, UVSOR activity report 1986, p62.
2) T.Ohba, S.Ikawa and S.Konaka, in preparation.

Kondo states of Ce-compounds : CeB_6, CeTe and $CeIn_3$

Y.S.Kwon, N.Sato*, H.Abe*, T.Nanba, S.Kunii, M.Ikezawa, T.Suzuki and T.Kasuya

Department of Physics, Tohoku University, 980, Sendai Japan
Department of Physics, Nagoya University, 464, Nagoya Japan*

CeB_6, CeTe and $CeIn_3$ among Ce compound show anomaly on the Fermi surface which is due to an localized electron existing in the 4f-shell. This phenomenon is called the dense Kondo effect. These are many reports on the anomaly in electric and magnetic behaviors on the Kondo substance. However the research of low energy optical properties have been rare. We measured the far infrared optical reflectivity of the single crystals of CeB_6, CeTe and $CeIn_3$ to obtain more detailed informations of the Kondo state, that is the electron structure of near Fermi surface.
The double reflection of 45^{o} incidence on sample surface for the photon energy from 10 to 200cm^{-1} has been measured on single crystals of CeB_6, CeTe and $CeIn_3$ at 10K and 300K (Fig. 1).
Fig. 2 shows the experimental results of the reflectivity at 10 and 300K for $CeIn_3$. There are simple Drude reflection due to the free electron appeared at 300K. An absorption, however, occured at about 6 meV at 10K. This absorption seems to correspond to the similar absorption already observed by us in Yb_4As_3[1] and CeBi[2]. This absorption differs from an optical phonon which appears at 20 meV from neutron scattering of $LaIn_3$[3]. The temperature of maximum (TM) electric resistivity of $CeIn_3$ is about 50K[4]. Therefore, this absorption seems to correspond to the Kondo Lattice formation. Fig. 3 shows the experimental results of the reflectivity at 10 and 300K for CeTe. In this case as $CeIn_3$ it can be seen only the Drude reflection due to the free electron also at 300K. An wide absorption centered at 14 meV, however, appears at 10K. TM from electric resistivity of CeTe is 30K[5]. The ordered magnetic moment per Ce atom is only $0.2u_B$[5]. It is suggested that CeTe at 10K has been already formed the Kondo Lattice. Therefore, this absorption seems to correspond to the Kondo Lattice formation. Fig. 4 shows the experimental results of the reflectivity at 10 and 300K for CeB_6. An absorption appears about 11 meV in the reflectivity at 10K comparing with that at 300K. Optical phonons from neutron scattering result appears above 23 meV[6]. The Kondo temperature (TK) of CeB_6 seems to be about 1K[7] . Even if CeB_6 at 10K is not yet formed the Kondo Lattice, this absorption seems to connect with Kondo effect. The absorption due to

Kondo peak near Fermi level is discovered in the far infrared optical reflectivity.

The detailed assignment needs more experimental studies, that is measurement under lower temperature (temperature of He^3) and high magnatic field.

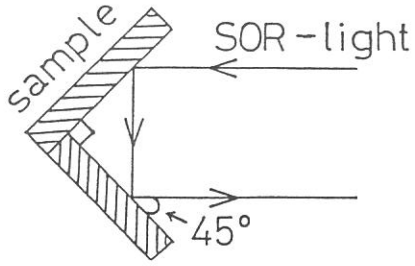

Fig.1. Method of the double reflection of 45° incidence on sample surface.

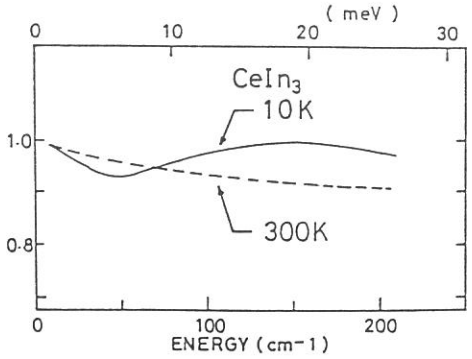

Fig.2. Photon energy dependence of the reflectivity for $CeIn_3$.

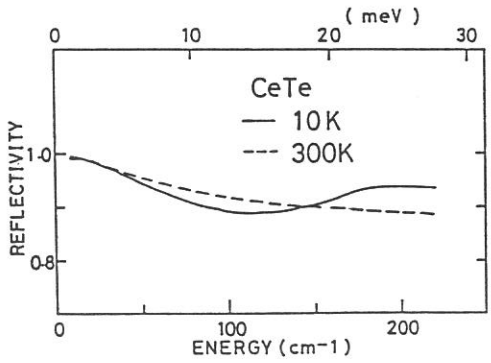

Fig.3. Photon energy dependence of the reflectivity for CeTe.

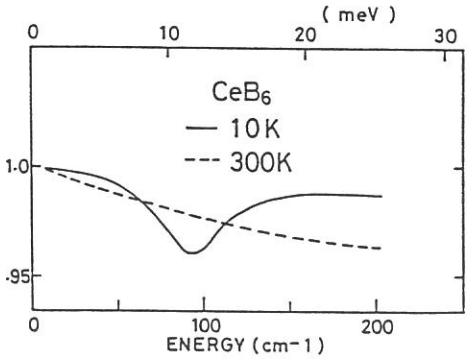

Fig.4. Photon energy dependence of the reflectivity for CeB_6.

[1] Y.S.Kwon, A.Ochiai, H.Kitazawa, N.Sato, H.Abe, T.Nanba, M.Ikezawa, K.Takegahara, O.Sakai, T.Suzuki and T.Kasuya, J. Magn. Magn. Mat. 70 (1987) 397-399

[2] Y.S.Kwon, A.Ochiai, H.Kitazawa, N.Sato, H.Abe, T.Nanba, M.Ikezawa, K.Takegahara, O.Sakai, T.Suzuki and T.Kasuya, Jpn. J. Appl. Phys. 26 (1987) Supplement 26, 539-540

[3] Y.Lassailly, S.K.Burke and J.Flouquet, J. Phys. C : Solid State Phys. 18 (1985) 5737-5747

[4] Q.Z.Gao, E.Kanda, H.Kitazawa, M.Sera, T.Goto, T.Fujita, T.Suzuki, T.Fujimura and T.Kasuya, J. Magn. Magn. Mat. 52 (1985) 286-288

[5] J.Schoenes and F.Hulliger, J. Magn. Magn. Mat. 63&64 (1987) 43-45

[6] H.G.Smith, G.Dolling, S.Kunii, M.Kasaya, B.Liu, K.Takegahara, T.Kasuya and T.Goto, Solid State Commun. 53 (1985) 15-19

[7] N.Sato, A.Sumiyama, S.Kunii, H.Nagano and T.Kasuya, J. Phys. Soc. Jpn. 54 (1985) 1923-1932

FAR-INFRARED ABSORPTION SPECTRUM OF SUPER IONIC CONDUCTOR $RbAg_4I_5$

Teruyoshi Awano, Takao Nanba,* Mikihiko Ikezawa* and Makoto Watanabe**

Department of Applied Physics, Tohoku Gakuin University, Tagajo 985
* Department of Physics, Tohoku University, Sendai 980
** Institute for Molecular Science, Myodaiji, Okazaki 444

The alkali silver iodide super ionic conductor $RbAg_4I_5$ has the highest room-temperature specfific conductivity, $0.27(\Omega\,cm)^{-1}$, of any ionic crystal.[1] Crystals of $RbAg_4I_5$ belongs to $P4_132$ or $P4_332$ at temperatures above 208K(α phase). They belong to R32 between 121.8K and 208K. Below 121.8K, they do not have high conductivity, and belong to trigonal, but details are not clear.

In the α-phase, the crystal contains four formura units per unit cell with 16 Ag^+ ions distributed over 56 interstitial sites forming two equivalent sets. These Ag^+ ions are in slightly distorted iodine tetrahedra.

The diffusive motion of Ag^+ ion is expected to give light scattering or absorption with energies of the order of a few cm^{-1}. The Raman spectrum of $RbAg_4I_5$ has been studied by Gallager and Klein.[2] But far-infrared absorption spectrum has not been studied in detail because of the experimental difficulties.[3]

We have measured reflectivity in region from 7 to $200cm^{-1}$ and calculated dielectric constants by the Kramers-Kronig transformation. Samples are prepared in iodide hydroacid solution saturated by RbI and AgI.[4]

Fig.1 shows the reflectivity spectrum and Fig.2 the imaginary part of dielectric constant. At 300K there are three main absorption bands near $80cm^{-1}$, $18cm^{-1}$ and $6cm^{-1}$. At 77K, under the phase transition temperature, the $6cm^{-1}$ absorption has disappeared, although the $18cm^{-1}$ peak, which is thought to be due to the diffusive motion of Ag^+ ion, has remained. This suggests that $6cm^{-1}$ absorption is due to the diffusive motion of Ag^+ ion. At 15K many peaks has begun to separate. Most of them seem to be doublets. This seems to be due to the tunneling effect among the equivalent sites. The peaks near $80cm^{-1}$ are similar and slightly shifted to those of Raman spectrum[2] and seems as TO-LO splitting. The assignment of these fine structures is left as a future problem. Also the the temperature dependence of the reflectivity nearby the phase transition temperature should be studied.

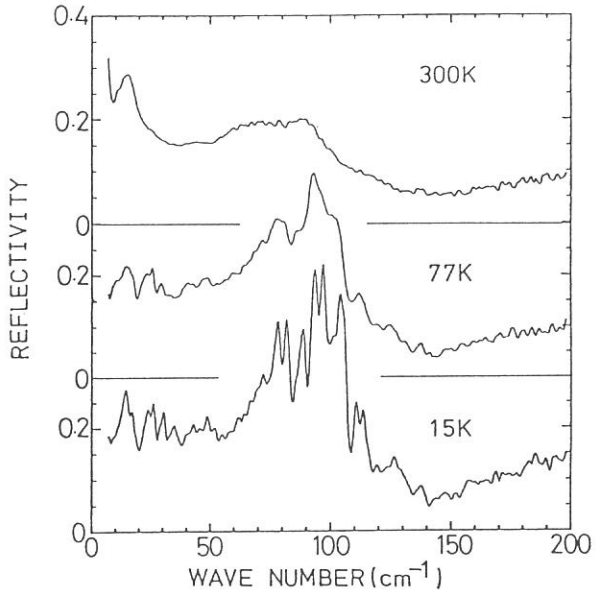

Fig. 1

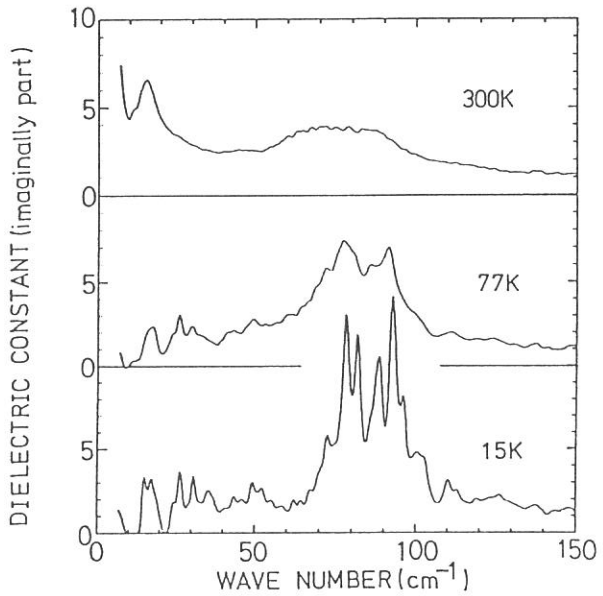

Fig. 2

1) B. B. Owens and G. R. Argue, Science 157, 308 (1967).
2) D. A. Gallager and M. V. Klein, Phys. Rev. B19, 4282 (1979).
3) K. Funke and H. J. Schneider, Solid State Ionics, 13, 335 (1984).
4) M. R. Manning, C. J. Venuto, and
D. P. Boden, J. Electrochem. Soc. 118, 2031 (1971).

MEASUREMENTS OF FAR-INFRARED SPECTRA OF MOLECULAR CRYSTALS

Hideyuki NAKAYAMA, Gako ARAKI, Ryoji HAGIWARA, and Kikujiro ISHII
Department of Chemistry, Gakushuin University,
Mijiro, Toshimaku, Tokyo 171

The far-infrared measuring system which has been installed at the beam-line BL6A by Namba et al.[1] was used for the measurement of the lattice-vibrational spectra of molecular crystals. The small spot-size of the measuring light as well as its polarization have been expected to be useful for the far-infrared measurement on solid state samples.

The cryostat was used with a small modification for the transmission measurement. Other equipments was used without modification. Thin single crystals cut from the Bridgman ingots were mounted on sample holders with 4mm apertures.

[1] Carbazole

Figure 1 shows (a) light intensity through the reference aperture, (b) light intensity transmitted through a carbazole crystal at liquid nitrogen temperature with the crystal a-axis parallel with the light polarization, and (c) the transmittance. The dips indicated by arrows at 73 and 128cm^{-1} in (a) arise from the absorption by the polyethylene window of the sample chamber and by the quartz window of the detector, respectively. Spectrum (c) almost agrees with the literature.[2] However, the intensity normalization by the reference is not perfect, since there remains a dip of absorption at 128cm^{-1} (arrow in (c)) where a single broad band is considered to exist. Thus, one must be careful in interpreting the fine structure of the spectrum.

[2] Phenothiazine

Phenothiazine has a ferroelastic transition at 248.8K, and Raman spectra in the lattice-vibrational region have been studied in detail.[3] Figure 2 shows the transmission spectra at room temperature (R.T.) and liquid nitrogen temperature (L.N.T.) with the polarization along a- and b-axes. Group theoretical analysis indicates that two lattice vibrational modes are infrared-active along these axes at room temperature, while four and five modes are active along a- and b-axes in the low-temperature phase, respectively. We recognize some prominent absorptions in

both the phases, but the noise of the base line prevent the identification of the weak bands.

1) T. Nanba et al., Int. J. Infrared and Millimeter Waves 7 (1986) 1769. 2) A. Bree and R. Zwarich, J. Chem. Phys. 49 (1968) 3344. 3) H. Nakayama and K. Ishii, Chem. Phys. 114 (1987) 431.

Fig. 2 Transmission spectra of phenothiazine

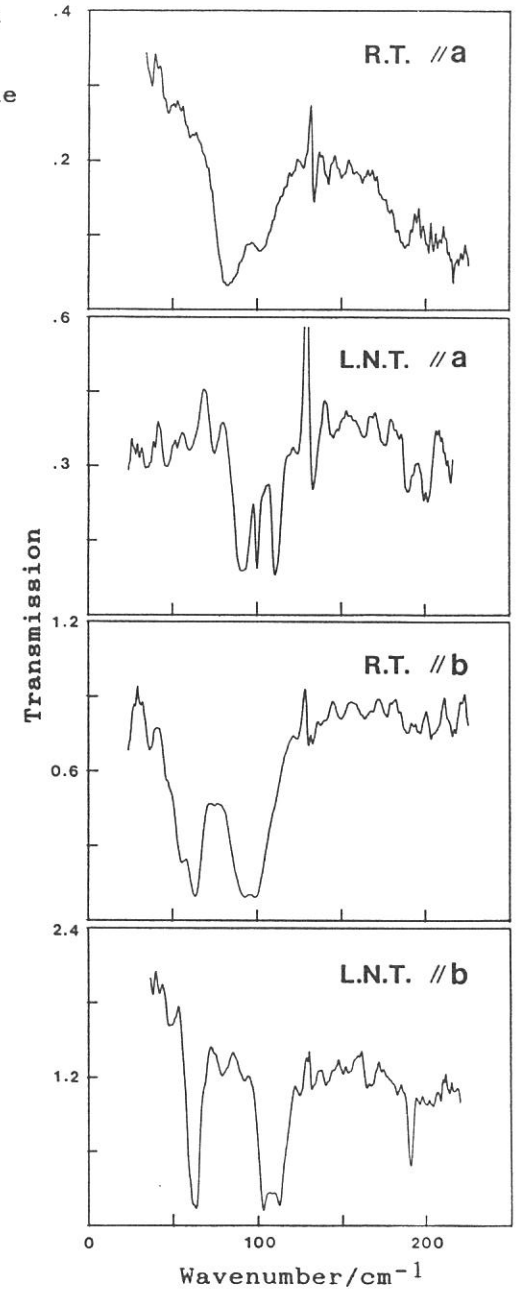

Fig. 1 Carbazole (a-axis) at liquid nitrogen temperature